Revista Română de Inginerie Civilă

Indexată în bazele de date internationale (BDI)

ProQuest, INSPEC, EBSCO

INDEX COPERNICUS, ULRICH'S şi JOURNALSEEK

Volumul 13 (2022), Numărul 2

MATRIX ROM
OP CHIAJNA CP 2
077040 – ILFOV
Tel. 021 4113617 Fax. 021 4114280
e-mail: office@matrixrom.ro
www.matrixrom.ro

Romanian Journal of Civil Engineering is founded, published and funded by publishing house MATRIX ROM
Executive Director: mat. Iancu ILIE

Online edition ISSN 2559-7485
Print edition ISSN 2068-3987; ISSN-L 2068-3987

Modelling Sustainable Urban Drainage Systems

Modelarea sistemelor de drenaj urban durabil

Alexandra Georgiana Ioan, Iulian Iancu, Anton Anton

Hydraulics, Sanitary Engineering and Environmental Protection Department,
Technical University of Civil Engineering of Bucharest, Bvd Lacul Tei no. 124, sector 2, 020396, Bucharest, Romania
E-mail: ioan.alexandra.georgiana@gmail.com, iulian.iancu@utcb.ro

DOI: 10.37789/rjce.2022.13.2.1

Abstract - In the recent years natural phenomena such as flood have cost billions of euros and numerous losses of human life. In this context, accurate modelling of storm runoff from urban catchments is very important, but it is difficult to achieve because of the complexity of modelling green areas. Depending on the local practice, the available software, the data availability, the possibility of data processing, computation time, and even the experience of the modeller, storm runoff from urban catchments can be analysed using different modelling approaches. Choosing the modelling approach, the rainfall loads to the model and the model parameters are very important steps that must be made with caution, and there is thus a need to establish more precise guidelines to help modellers in choosing the most suitable modelling approach. The overall objective of the research project is to investigate the possibilities of managing the storm water to cope with climate change in a sustainable way. The storm water can be used as a resource, as an element in urban recreational activities. This initiative is supported by the key principles of sustainability: water recycling, minimizing pollutants in storm water and urban environmental protection against flood events.

Index Terms - 1D modelling, Climate Change, Sustainability, SUDS

Introduction

Over the next decades, extreme weather events are expected to become even more frequent due to climate changes (Arnbjerg-Nielsen, Leonardsen, & Madsen, 2015). The extent and nature of expected changes varies across the globe. In the past 30 years, changes in rain patterns have been observed in Denmark in terms of extreme precipitation. These changes are mainly visible in the frequency of extreme events, but there is also a tendency for an effect on their magnitude (Arnbjerg-Nielsen, 2012). There are different approaches to adapt cities to these extreme events. One approach is the

conventional adaptation where the sewer system is enlarged, but this is not always possible due to very big implementation costs. Another approach is adapting the urban landscape for stormwater management, which is often called Low Impact Development (LID) or Sustainable Urban Drainage Systems (SUDS) and involves elements of Green Infrastructure (GI) (Fletcher et al., 2014). There are several possibilities to 'reconstruct' the cities considering the space needed for stormwater. This will allow the cities to redirect the stormwater to areas that are designed and suitable for flooding, inside or outside the cities, during extreme rain events. This approach has become increasingly popular in Denmark over the past few years (The City of Copenhagen, 2015).

Materials and methods

The presented research is applied to the area of Trekroner Øst (Figure 1), located in Roskilde municipality, at 28km west of Copenhagen where the storm water system was designed based on the principals of sustainability. The research presented here focuses on the complexity of modelling stormwater movements in urban catchments during extreme events with an emphasis on the consideration of green areas and SUDS's. The flood modelling approach is developed and tested using the MIKE 2016 software package (DHI, 2016). Storm runoff from urban catchments is modelled by considering green areas using Horton's equation (eq. 1) where infiltration is an exponentially decaying process with large infiltration capacity in the beginning of the event.

$$I_H(t) = I_{Imin} + (I_{Imax} - I_{Imin)}. e^{-k_a.t} \qquad (1)$$

where:

$I_{H(t)}$ Horton infiltration (m/s);
I_{Imin} initial (maximum) infiltration capacity (m/s);
I_{Imax} final (minimum) infiltration capacity (m/s);
K_a empirical constant (time factor) (s^{-1});
t time since the rainfall starts (s).

The storm runoff from green areas is included in the runoff model as a runoff that loads the drainage system. In Denmark the adopted modelling approach is to consider both paved and green urban areas through an initial loss in the runoff model a fact that may generate unrealistically loading of the sewer system if the runoff from this type of areas becomes a significant part of the total runoff model (extreme events).

The Trekroner Øst catchment is divided into 40% flat impermeable areas and 60% permeable areas with an average infiltration capacity. Impermeable areas such as

roofs, roads and parking areas are reduced by the initial losses divided into: $5x10^{-5}$m initial losses in wetlands and $6x10^{-4}$m initial losses stored. The runoff from Impermeable areas is also reduced by initial losses: $5x10^{-5}$m initial losses in wetlands and $4x10^{-2}$m initial losses stored. The soil type is clayey and based on the infiltration parameters in the literature, the maximum infiltration capacity has been established $5x10^{-5}$m/s and will be reduced during the rain event to $1x10^{-6}$m/s. Non-perishable surfaces are divided into steep surfaces (roofs) and flat surfaces (parking lots) while the permeable areas are divided into permissible areas where the infiltration capacity is high, medium and small. In this study for ease of calculation the assumption is that all non-perishable surfaces in the model are flat and all permeable areas have an average infiltration capacity. This method allows to consider infiltrations for permeable areas where infiltrations decrease exponentially. A high infiltration capacity at the beginning of the precipitation event is also considered. For this conceptual model, the properties of the soil are represented by the input parameters.

Figure 1: Trekroner Øst area

Mathematical modelling

The research study will be concentrated only on the possibilities of modelling the storm water system where the urban landscape is used for the storm water management. The software that will be used for this research study is the MIKE suite by DHI (Danish Hydraulic Institute). MIKE URBAN will be used to describe the collection of storm water and water flow to the sewer system. The model will describe the drainage system structure, reservoirs, swales, open channels, etc. In MIKE URBAN the hydrological units are represented by catchments, where the storm water and the infiltration are generated based on different sets of parameters for each unit. It will be used a one-dimensional model to get a better understanding of the connection between the surcharged drainage network and overland urban flooding, to give a clear overview of the locations of flooding. The mathematical model will be used to simulate the hydrology and the hydraulics of the implemented Sustainable Urban Drainage Systems.

When the area was constructed the space for the storm water was considered, the storm water drainage became an urban component, allowing the area to be prepared for redirecting the storm water to areas outside the project area largely on the surface. To simulate this in the analysis both hydrological and hydraulic models used in this research were validated and calibrated based on in situ measurements. A rainfall-runoff model which consists of a hydrological model and a hydraulic model was created to forecast the future situations in the newly constructed drainage system. The model will be calibrated based on in situ measurements. Quantitative data such as rainfall, flow and water levels were recorded to perform a calibration of the model.

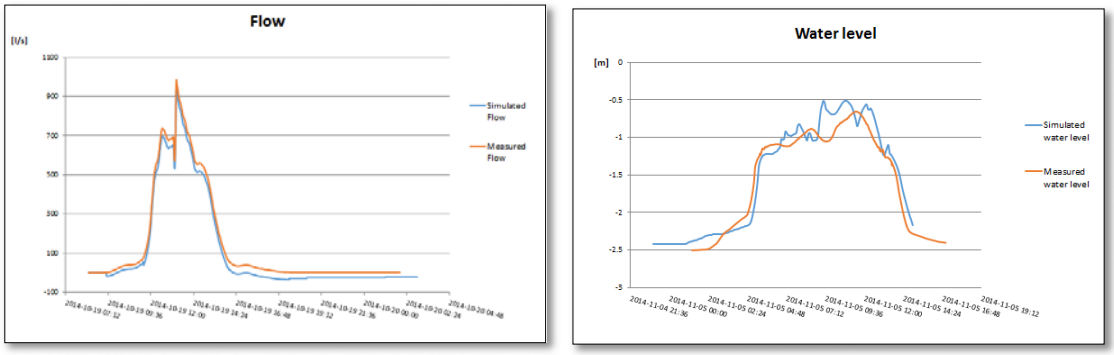

Figure 3: Calibration showing flow results / water level results

After the calibration, the mathematical model was able to recreate a similar flow/ water level model as the measured flow / water level shows. The requirement of the calibration was that the error in volume may be up to 10% and the error in peak flow may be up to 10%.

After the calibration and validation, the mathematical model was used to analyse the capability of the Sustainable Urban Drainage Systems to retain and transport different rain events. Several types of Sustainable Urban Drainage Systems have been implemented in the area: swales, bio retention areas, grassed or paved open channels, etc., presented in Figure 2:

Figure 2: The Trekroner Øst catchment (a) and storm water management (b)

After the validation, the model was used to analyse rain events measured in the stations close to the project area: 5855 (ROSKILDE NAVERVÆNGET PE3) and 5840 (ROSKILDE NYMARKEN OB8). A long time simulation (LTS) based on 20 years historical rain events was performed in order to validate the model and the Sustainable Urban Drainage Systems contribution.

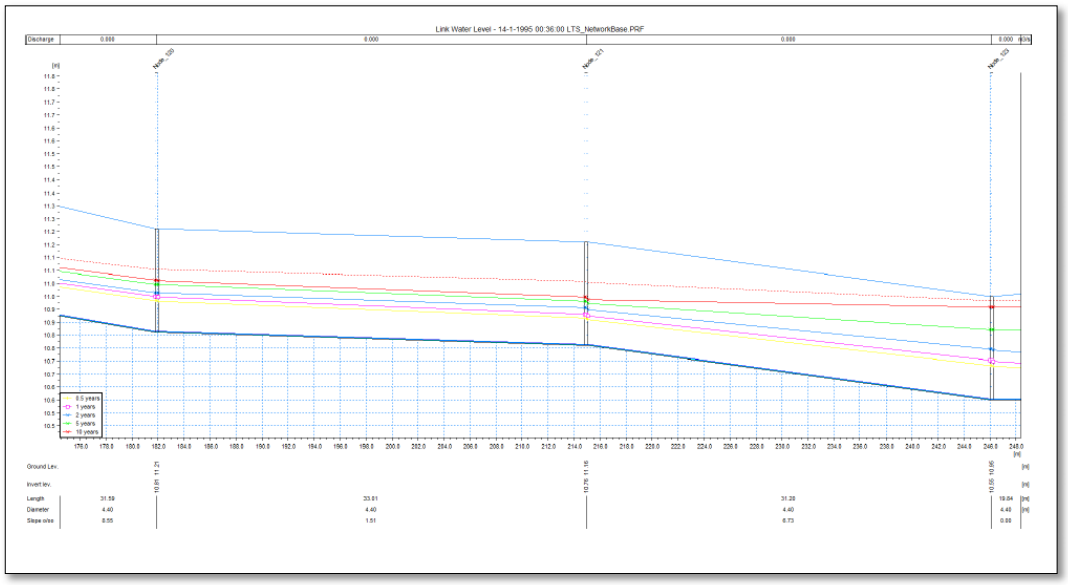

Figure 3: The water level results for a part of the Trekroner Øst sewer system

The mathematical model was also used for flood computations. There was defined four scenarios that represent different predictions of future rain events, considering the predicted increase in precipitations, in order to evaluate the drainage system's capacity and future function. The proposed events are the 5-year event, the 10-year event, the 20-year event and the 50-year event. For the calculation of statistical rain with a a 10-year

event, the latest version of the Skrift 30 guide was used. In this version are presented the average annual precipitation (the number of extreme events) and the average daily extreme precipitation (magnitude of events) according to the regional climate model (1989-2010). In the statistical calculation, the research area is identified on the basis of the coordinates x (east) - y (north) where the ETRS 1989 UTM ZONE 32N coordinate system is used. Once the area is identified, average annual rainfall and average daily rainfall are automatically identified from the database.

Results and discussion

Based on the expected significant increase in the frequency and intensity of precipitation, the research presented in this article address the hydraulic and hydrological modelling of urban basins. The calibration of the mathematical model was carried out exclusively taking into account the hydrological parameters that directly influence the amount of rainwater discharged into the sewer system. The target of this calibration was that the volume and maximum errors recorded to be up to 10%, and the correlation coefficient (R) to be between 0.8 - 1. All events were calibrated separately, and the analysis performed on the runoff parameters resulted in values that matched in more than 50% with the recorded events. In order to determine the water flows transported by the sewer system, the hydrological reduction factor, the concentration time and the initial losses as recommended in the literature were taken into account, thus making it possible that after calibration, the model would be able to convey a transported flow rate and a depth of water in the channel similar to the measured data. Climate change has a significant impact on the urban environment, so it was important to develop a mathematical model that would be able to reproduce present situations in terms of precipitation. After the mathematical model of the sewer system was calibrated, it was used to analyse the consequences of increasing the intensity of precipitation due to climate change. The results showed that the permeable areas the rains cannot infiltrate completely on extreme events and that the Sustainable Urban Drainage Systems are helping the sewer system to cope the extreme events rainwater volumes.

Acknowledgement

We are grateful to Henrik Sønderup (Head of Department, Climate Adaptation and Landscape Architecture, Rambøll Denmark) for providing the input data and all the software used in this research.

References

Arnbjerg-Nielsen, K. (2012). Quantification of climate change effects on extreme precipitation used for high resolution hydrologic design. Urban Water Journal, 9(2), 57–65. http://doi.org/Doi 10.1080/1573062x.2011.630091

Arnbjerg-Nielsen, K., Leonardsen, L., & Madsen, H. (2015). Evaluating adaptation options for urban flooding based on new high-end emission scenario regional climate model simulations. Climate Research, 64(1), 73–84. http://doi.org/10.3354/cr01299

DHI. (2016). Runoff Reference manual, 1– 50.

Fletcher, T. D., Shuster, W., Hunt, W. F., Ashley, R., Butler, D., Arthur, S., … Viklander, M. (2014). SUDS, LID, BMPs, WSUD and more – The evolution and application of terminology surrounding urban drainage. Urban Water Journal, 9006(September), 1–18. http://doi.org/10.1080/1573062X.2014.916314

The City of Copenhagen. (2015). Climate Change Adaptation and Investment Statement - Part 1, (October).

Specific conditions for an optimal operation of air-water heat pumps

Condiții specifice pentru o funcționare optimă a pompelor de căldură aer-apă

George Dragomir, Ioan Boian

Universitatea Transilvania din Brașov,
B-dul Eroilor 29, Brașov, România

e-mail: boian.ioan@gmail.com, segadproiect@gmail.com

DOI: 10.37789/rjce.2022.13.2.2

Abstract. The paper presents conditions required for an optimal operation of air-water heat pumps used for space heating and cooling. Designing such an installation able to reduce the greenhouse gas, *GHG* emission involve a prerequisite envelope improvement: its thermal performance is in a correlation with the seasonal performance factor, *SPF* resulting from the climatic conditions and from the heat pump setting having the primary energy factor, *PEF* together with the specific emission index for electricity generation, I_e as influencing factors. At the same time, the type of the fuel, (gas, coal, etc.) i.e., its *GHG* emission intensity, I_f and the efficiency, η_c of the original boiler that is to be replaced with the heat pump are important when analyzing the performance that can be achieved after this replacing. For air-water heat pumps an operation under the air temperature of +7 ºC seems to be not advisable from the efficiency and from the power consumption point of view.

Key words: air-water heat pumps

1. Introduction

Climate change, the result of global warming is evident by the increasingly frequent excessive phenomena: this increase of the global temperature is caused by the greenhouse gas emissions, *GHG* the main factor being carbon dioxide, CO_2. Energy "hunger", visible on a global scale, is an effect of the economy development: it requires an energy conversion, traditionally obtained through the burning process of fossil fuels.

Studies and research concerning the *GHG* emission from fossil fuels burning have been carried out in Europe and around the world having in mind that internal combustion engines and equipment used to provide thermal comfort in buildings are based on such burning processes. In Europe and beyond, buildings are the main energy consumer, i.e., about 40 per cent of the total energy is used by the building sector, being responsible of approx. 36 per cent of the CO_2 emission. Therefore, limiting the increase of the global temperature to 1.5 ^oC, set out in 2015 by the Paris Agreement, at COP21, in order to avoid a worsening of the effects due to climate change, involves an annual reduction of *GHG* emissions by 7.6% by 2030. It must be noted that global efforts to achieve this goal have so far proved insufficient. Decarbonization - including measures to reduce *GHG* emissions, aims to reduce and limit global temperature rise. Recently, on 14 July 2021, the European Commission proposed a package of measures on climate, energy, land use, transport and taxation policies to transform the EU economy and society in order to achieve climate ambitions, entitled *European Green Deal*: these policies aim to reduce net greenhouse gas emissions by at least 55% by 2030 compared to 1990 levels. This will facilitate the necessary acceleration of measures aimed at reducing *GHG* emissions in the next decade by combining policies such as the application of emissions trading in new sectors with the tightening of the existing emissions trading system in the EU, along with an increased use of renewable energy sources and together with an improved energy efficiency, etc.

In fact, the UN Summit "COP 26" on climate change held in Glasgow, in the autumn of 2021 took into account the fact that "it is necessary for every company, every financial firm, every bank, insurer and investor to change in order to achieve our climate goals". This implies a wide financial mobilization: "we all have a role to play in combating climate change", the involvement of cities, regions, companies, investors and universities is needed. Achieving the proposed target i.e., limiting the increase in global temperature to 1.5 ^oC - implies an annual decrease in fossil fuel production of 6% for the current decade, while increasing the contribution of renewable energy. While 91% of the electricity currently generated is of solar and wind type (over 80% of new capacities appeared in 2020 were renewable), in the transport and in the space heating sector there has been a much slower progress or even a lack of the this progress.

Achieving climate change targets by the reducing of *GHG* emissions involves a significant change in the way they are heated and cooled. In this context, an increasing number of heating / cooling installation projects based on heat pumps and especially those that use atmospheric air as a source can be noted, given their attractiveness resulting from price, installation effort and commercial promotion.

It is therefore of interest to specify appropriate requirements that can ensure the optimal operation of these installations based on air-to-water heat pumps.

2. Energy performance of the envelope

Until recently it was considered within the EU, that limiting global temperature rise and reducing *GHG* emissions by 40%, respectively, could avoid the disastrous effects of climate change. In order to achieve a climate neutrality by 2050 the European Commission has set an intermediate step for cutting the *GHG*-emissions at least 55% by 2030. This package of proposals was launched mid-summer of 2021 under the name "Fit for 55" [1]. Even so, it has been scientifically proven that this target is still far from the level needed to limit the catastrophic impact specific to a global temperature increase of 1.5 ^{o}C.

The mitigation of *GHG* emissions resulting from the burning of fossil fuels implies a reduction of energy consumption, mainly related to the heating and air conditioning of indoor spaces. This can be done through an improvement of the energy performance of the building envelope: the *energy consumption index* for heating, will be diminished from the current value $\boldsymbol{C_e}$ [kWh$_{heat}$ / (m^2 year)] to a lesser-one, $\boldsymbol{C'_e}$ i.e., $\boldsymbol{C'_e < C_e}$**.** Increasing the energy performance of the envelope paves the way for the replacement of equipment based on the burning of fossil fuels, such as the boiler, with alternatives such as the heat pump. Considering the level of CO_2 emissions [kgCO_2/(m^2 year)] in case of a boiler $\boldsymbol{E_{GHG}^{boiler}}$ and that of the heat pump $\boldsymbol{E_{GHG}^{hp}}$ the *relative reduction of GHG emissions compared to 1990*, $\boldsymbol{RRE_{GHG}^{1990}}$ is,

$$RRE_{GHG}^{1990} = \frac{E_{GHG}^{boiler} - E_{GHG}^{hp}}{E_{GHG}^{boiler}} \quad (1)$$

The *GHG emission level intensity* of the boiler $\boldsymbol{E_{GHG}^{boiler}}$ depends on the *energy consumption index for heating* $\boldsymbol{C_e}$ and on *CO_2 emissions factor* specific for the fossil fuel used by the boiler, $\boldsymbol{I_f}$ [g $CO_{2\ eq}$/kWh$_{heat}$], and on the *efficiency of the boiler,* $\boldsymbol{\eta_b}$

$$E_{GHG}^{boiler} = \frac{C_e}{\eta_b} I_f \quad (2)$$

In case of the heat pump the *GHG emission level* $\boldsymbol{E_{GHG}^{hp}}$ is related to the *energy consumption index for heating* the space having an improved energy performance of the envelope $\boldsymbol{C'_e}$ and to the *GHG emission intensity of electricity generation* $\boldsymbol{I_e}$ [g $CO_{2\ eq}$/kWh$_{el}$], and to the *seasonal performance factor SPF* of the heat pump

$$E_{GHG}^{hp} = \frac{C'_e}{SPF} I_e \quad (3)$$

Combining (1) with (2} and {3) a *relative reduction of the specific energy consumption* $\boldsymbol{C'_e/C_e}$ can be derived in correlation with characteristic elements of the boiler $\frac{I_f}{\eta_b}$ and that one's of the heat pump $\frac{I_e}{SPF}$, and with the relative emission reductions $\boldsymbol{RRE_{GHG}^{1990}}$

$$\frac{C_e'}{C_e} = \left(1 - \boldsymbol{RRE_{GHG}^{1990}}\right) \frac{I_f}{\eta_b} \frac{SPF}{I_e} \quad (4)$$

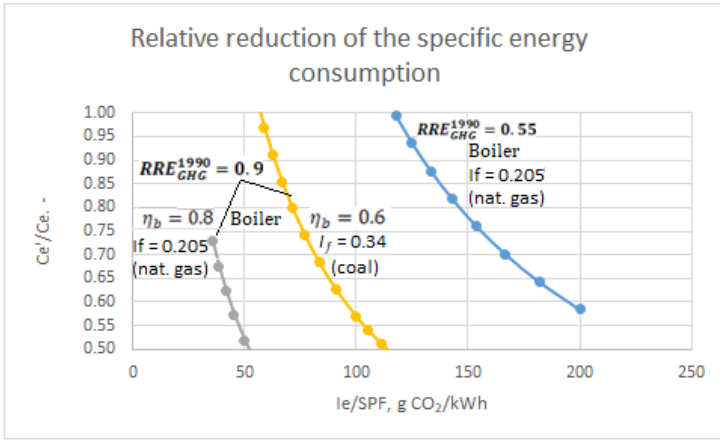

1.a. The relative reduction of the specific energy use of a building as a function the heat pump characteristic elements, and having the boiler characteristic elements as paramethers.

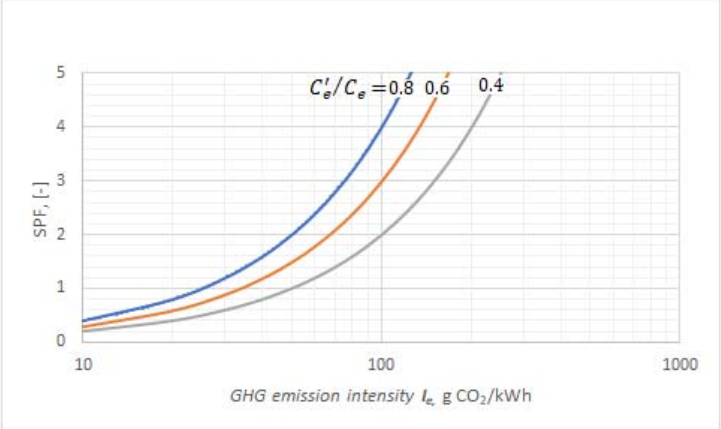

1.b. The seasonal performance factor of a heat pump necessary to be achieved for the 2050 condition depending on GHG emission intensity and on the relative reduction of the specific energy use as a paramether.

This correlation, presented in Figure 1a, shows that the target established through the project "Fit for 55" is feasible for the period until 2030 even if a 80%-efficiency, natural gas-boiler is to be replaced by a heat pump working with a $\boldsymbol{SPF > 2{,}5}$ when the electricity used for its electromotor is generated with a *GHG emission intensity* $\boldsymbol{I_e < 500}$ **g CO_2/kWh** ($I_e/SPF \leq 200$). In this situation a minimum 40 % relative reduction of the energy consumption resulting from an improvement of the building envelope is necessary: it corresponds to $\boldsymbol{C_e'/C_e \geq 0{,}6}$, that is a common situation.

On the other hand, under the conditions provided for 2050, as shown in Figure 1b, a relative emission reduction of $\boldsymbol{RRE_{GHG}^{1990} = 0.9}$ needs a heat pump working with a $\boldsymbol{SPF > 3}$ when the supplied electricity was generated with a *GHG emission intensity* $\boldsymbol{I_e \leq 150}$ **g CO_2/kWh**, (I_e/SPF≤50): in such a situation the envelope must be insulated and sealed to get an improvement of 50% or higher for the *relative reduction of the specific energy consumption,* $\boldsymbol{C_e'/C_e \geq 0.5}$.

3. Electricity as a CO_2 generator

Usually heat pumps and those used in the residential sector are driven by electromotors i.e., electricity is required for their operation, resulting in *GHG* emission, as any technology used for the generation is responsible for this emission. In case of fossil-fueled generation the carbon footprint is higher than that of a renewable and nuclear process: *GHG* is produced in traditional electricity generation during the power plant operation, and not upstream of operation, i.e., during the construction phase of the plant, being an indirect emission. As a result, the *GHG emission intensity of electricity generation* $\boldsymbol{I_e}$ is a country- characteristic, as shown in Figure 2. It can be noted, that while in Scandinavian countries the values for the *GHG* emission are very low, under

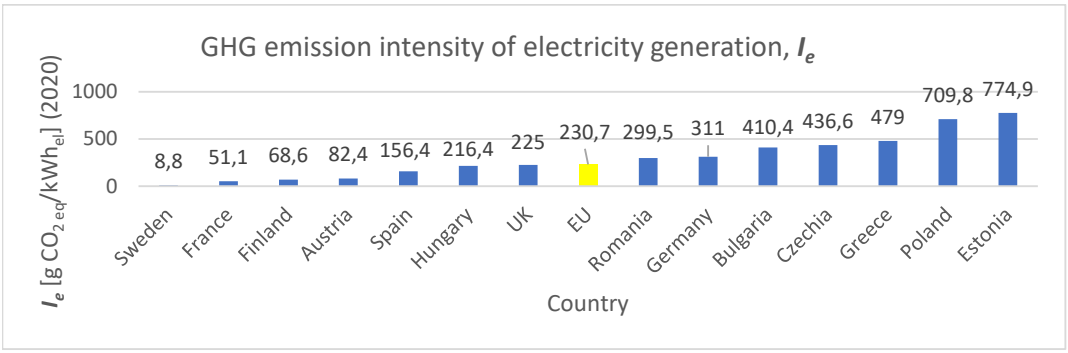

Fig.2. GHG emission intensity of electricity generation, I_e by country, in EU, 2020 [3]

50 g CO_2 -eq/kWh (even under 10, specific for hydroelectric, wind and nuclear) in the Central European area higher values of approx. 500 g CO_2 -eq/kWh (or even more) are still current (specific for natural gas and coal).

The general trend of the *GHG emission intensity of electricity generation* $\boldsymbol{I_e}$ is a downward one, and for 2030 the indicative level in EU is forecasted to be in the range of 110 to 118 g CO_2 -eq/kWh, as shown in Figure 3.

Reducing the *GHG* emission depends on the paradigm change, meaning a replacement of the traditional fossil-fuel based technologies with renewable-ones, as the solar-one release about 20 times less *GHG* than those coal-fired.

Beyond the generation of electricity and the associated *GHG* emission, it is necessary to consider its transport and distribution with the accompanying losses. The

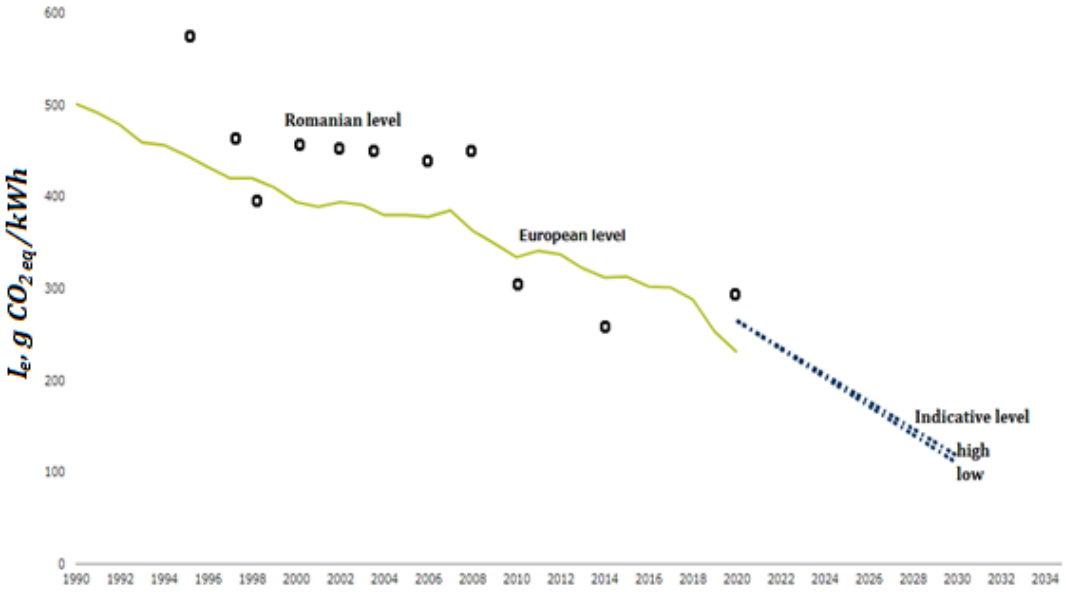

Fig.3. The progress of *GHG emission intensity of electricity generation, I_e* for the last three decades in EU, and with the 2030-prevision. Some values for Romania are indicated too [3].

Primary Energy Factor, PEF is defined as the raw primary energy required to provide for the electricity generation divided by the delivered electricity. *PEF* takes into account energy losses occurred during its production, transport and distribution. The efficiency of the entire process, η_{tot} is the reverse of the *PEF*

$$\eta_{tot} = 1/PEF \qquad [5]$$

EUROSTAT has established for the EU a value of *PEF* = 2.5, which correspond to $\eta_{tot} = 0.40$. Recently, as the share of renewable energy sources *RES* has increased from 14,8% in 2005 to 30% in 2017 and a value of 49% being predicted for 2030, a lower *PEF* value was proposed. A detailed analysis carried out by COGEN Europe says that the revised value of *PEF* to be used in the framework of the Energy Efficiency Directive, *EED* for the period post 2020 should not be lower than **2.3** [3], leading to a mean efficiency of the power system of $\eta_{tot} = \mathbf{0.43}$. In fact, for the period 2018 - 2050 a linear increase of the efficiency is foreseen, so that at the end of this interval it reaches the value of $\eta_{tot}^{2050} = \mathbf{0.45}$ corresponding to a *PEF* = **2.22**.

4. Operating performance of the heat pump

The *seasonal performance factor, SPF* as the operating performance indicator of a heat pump working in a heating system is defined as the ratio of the total heat supplied to a building to the electricity used by the electromotor driving the compressor of this

equipment, both of the energy amounts evaluated for the whole season. Considering the ANNEX VII from the DIRECTIVE 2009/28/EC [4], "Only heat pumps for which

$$SPF > 1{,}15 * 1/\eta \quad [6]$$

shall be taken into account in case of aerothermal, geothermal or hydrothermal heat pumps". The mean efficiency, η is calculated as an EU average based on Eurostat data, i.e., the ratio between total gross production of electricity and the primary energy consumption for electricity production. For the period post 2020 having a mean efficiency of the power system $\eta = \mathbf{0.43}$ a limit value for the seasonal performance factor *SPF* results: ***SPF* >2.65** as shown in Figure 4. This means that values of *SPF* from the red area are not accepted for an optimal heat pump operation.

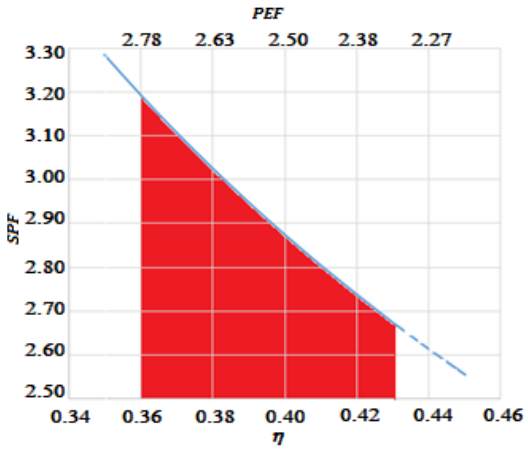

Fig.4. The correlation established by ANNEX VII, DIRECTIVE 2009/28/EC [4] between the seasonal performance factor *SPF* and the mean efficiency of the power system, η

SPF being a global indicator for the entire heating season do not reflect the influence of the momentary operating factors like the temperature of the source and that of the heated water supplied to the building by the heat pump. The *carnot coefficient of performance*, COP_{canot} is defined by these temperatures, that of the source - air in this case, T_{air} and that of the water supplied by the heat pump, T_w

$$COP_{carnot} = \frac{T_w}{T_w - T_{air}} \quad [7]$$

Higher values of COP_{canot} are possible only in cases when the temperature of water supplied by the heat pump is kept as close as possible to the source temperature, i.e., that of the air, as shown in Figure 5.

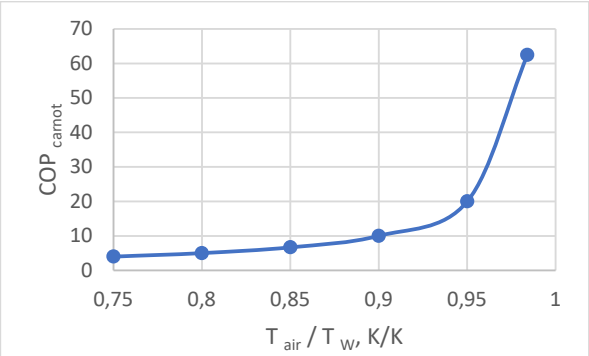

Fig.5. COP_{carnot} as a function of the temperatures ratio, the source one, T_{air} and water one, supplied by the heat pump, T_w.

The actual values of the coefficient of performance COP_{actual} are calculated as the ratio of the thermal power, P_{th} supplied by the heat pump and the electric power, P_{el} absorbed by its electromotor

$$COP_{actual} = \frac{P_{th}}{P_{el}} \quad [8]$$

In practice it is found that COP_{actual} is considerably smaller than the corresponding COP_{canot}

$$COP_{actual} < COP_{carnot} \quad [9]$$

This is due to the losses caused by the constructive-technological and operational factors that are described by the *exergetical coefficient of performance,* COP_{ex}

$$COP_{actual} = COP_{carnot} \cdot COP_{ex} \quad [10]$$

Usually, $COP_{ex} < 0.7$ and for heat pump capacity smaller than 20 kW, $COP_{ex} \approx 0.3 \ldots 0.5$, depending on the operating mode. Figure 6 shows the influence of the temperature of the water exiting the heat pump, T_w on the *exergetical coefficient of performance,* COP_{ex}, having as a parameter the temperature of the air at the entrance of the heat pump, T_{air}, for an equipment currently existing on the market. It is important to note that losses increase as the temperature of the air as a source rise from 7 °C to 20 °C, leading to a decrease of the maxCOP_{ex} from 0.41 to 0.30, as shown in Figure 6a. Similarly, when the air-temperature decrease from -7 °C to -20 °C a lowering of the maxCOP_{ex} from approx. 0.35 to 0.29 can be observed in Figure 6b. But even in the temperature range of +7 °C…-7 °C a diminution of maxCOP_{ex}, from 0.41 to 0.31 takes place, with the lowest values corresponding to a temperature close to 0 °C.

Improving the performance of a heat pump is an important step to win users / customers while choosing an equipment. That is why manufacturers assist air-source heat pumps with an electrical resistor to compensate the heat in case of low air-temperature. At the same time, controlling the flow of the thermal agent in the heat pump circuit by means of an inverter is able to adapt the heat supplied by the equipment to the heat use of the building.

An optimal operation of air-source heat pumps will avoid air- temperature close to 0 ºC in order to prevent water condensate, or even snow/ice deposit on the evaporator, as the heat transfer from the air to the thermal agent of heat pump is more difficult resulting in a supplementary cost. Data resulted from tests show that the maximal values of COP_{carnot} and COP_{ex} correspond to water temperature supplied by the heat pump in the range of 40 ºC.

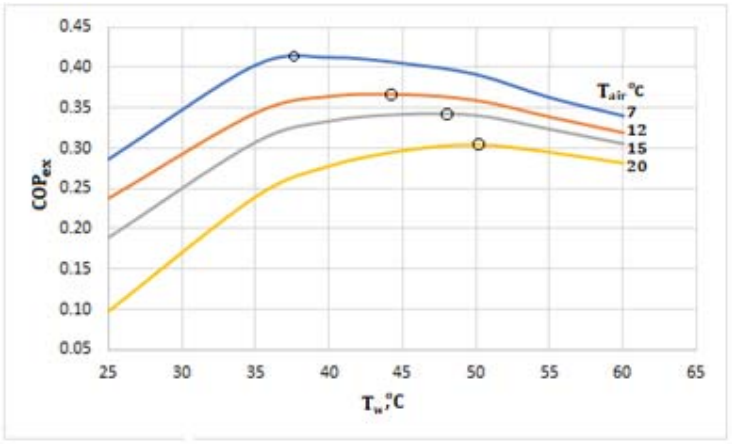

a)

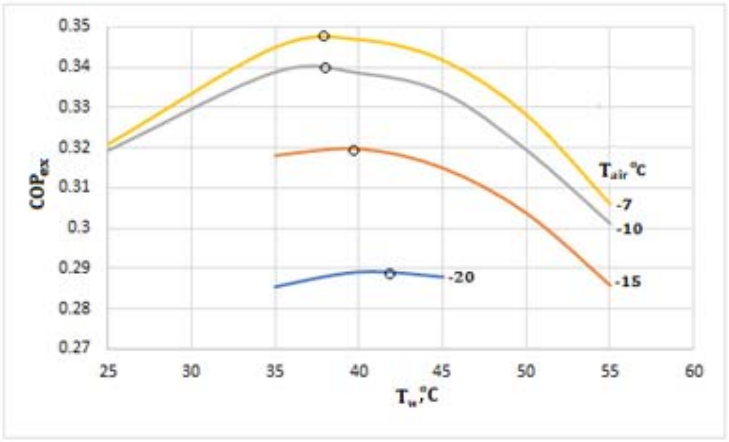

b)

Fig.6. The influence of the hot water temperature at the exit of the heat pump, T_w on the exergetic efficiency of the heat pump, COP_{ex}, with the air temperature at the entrance to the equipment, T_{air} as a parameter.

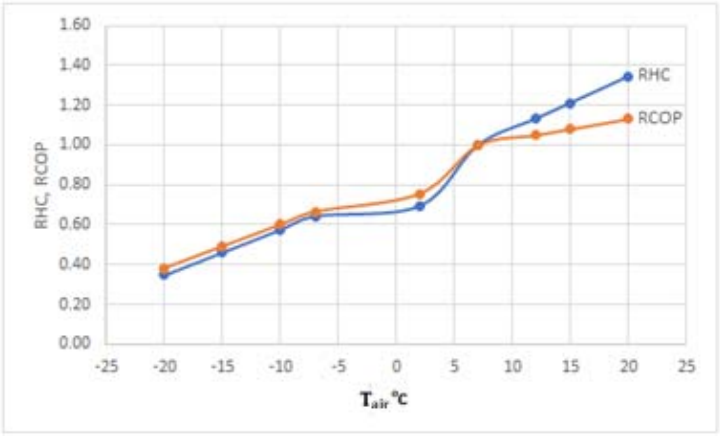

Fig.7. The relative heating capacity, *RHC* and the relative efficiency, *RCOP* on the air temperature T_{air}.

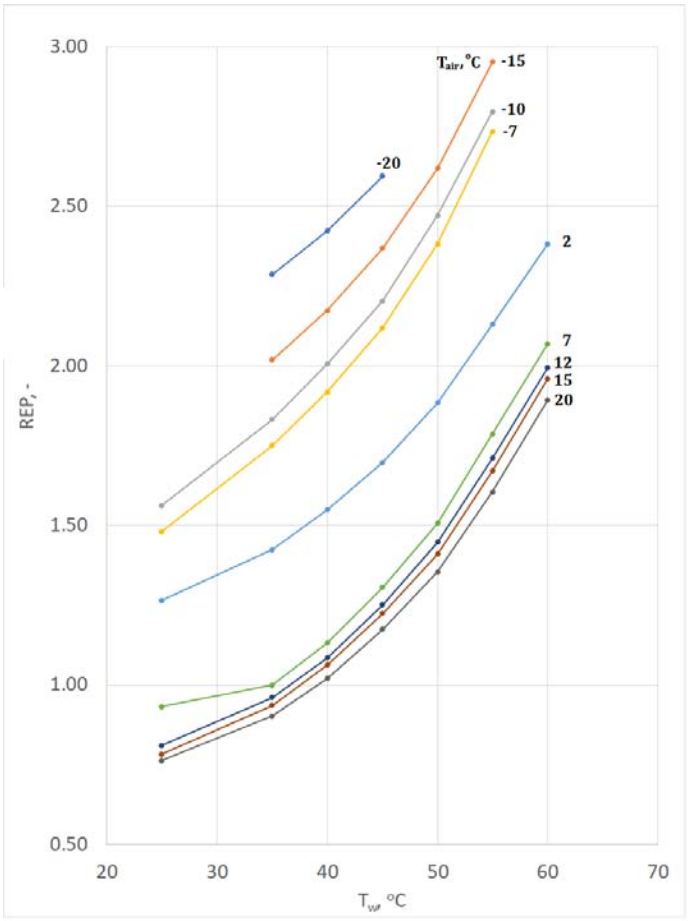

Fig.8. The relative electric power, *REP* correlated with the water temperature supplied by the heat pump and having the air temperature T_{air} as a parameter.

Moreover, air temperature under +7 ºC will cause besides a lowering of the *COP* a significant reduction in heating capacity. To estimate such effects, it is useful to compare the heating capacity with that specific for +7 ºC air temperature, the so-called *relative heating capacity, RHC.* Similarly, can be defined the *relative electric power, REP* and the *relative COP, RCOP.* Figure 7 shows the relative characteristics, *RHC* and *RCOP* resulted from specifications presented by data books of heat pumps currently existing on the market. It can be noticed, the most unfavorable air temperature interval, especially for *RHC* and *RCOP* decline, being between +7 ºC and +2 ºC, so that at +2 ºC *RHC* is diminished to 0.7 or *RCOP* to 0.8 compared to unity existing at +7 ºC. This trend continues when the air temperature drops, so at -20 ºC *RHC* and *RCOP* become almost one third of that measured at +7 ºC.

The analysis of data resulted from tests concerning the *relative electric power*, *REP* presented in Figure 8, shows

that air temperatures over +7 ºC will have a small influence, i.e., a reduction of *REP* from 10 to 20 %. However, the required temperature of the water delivered by the heat pump is of greater importance: when raising it from 35…40 ºC to 60 ºC this will double the electric power (the *REP* is becoming 2 instead of approx. 1). But when the air temperature drops from +7 ºC to -15 ºC or even -20 ºC a significant increase in *REP* will result, i.e., 150 % to 200 %, and even more, if the water temperature is in the range of 35…40 ºC. This increase in *REP* values will reach 300 % in case of a required water-temperature T_w of 60 ºC.

5. Conclusions

Mitigation of *GHG* emissions aimed at limiting them in order to avoid the devastating effects of global warming requires urgent enforcement measures. Carbon dioxide, the main cause of global warming, is the result of fossil fuel combustion processes requiring the replacement of heating equipment based on this principle.

In this context, the heat pump can be an attractive solution, and the air-water variant is often presented as a "miraculous" answer, especially in the conditions of a partial knowledge of the specific operating conditions. Mitigation the *GHG* emissions with 55% by 2030 and at least with 90% by 2050 are landmarks for the limitation of the global temperature raise at 1.5 ºC. The evaluations presented in the paper highlighted the need to reduce the specific energy use, primarily due to the improvement of the energy performance of the building envelope: reducing specific energy / heat use by 30% ... 50% is a feasible goal with current technologies and materials. Under these conditions, replacing a boiler based on fossil fuels (coal, liquid fuel, or natural gas) with an electrically operated heat pump can easily meet the condition of 55% reduction in GHG emissions if its operation is characterized by *SP*F> 2.5 and if the electric power used by its electric motor is generated under a specific emission index I_e < 0.5 kg CO_2 / kWh. However, the 90% reduction in *GHG* emissions set for 2050 imposes stricter conditions for both the heat pump, namely SPF>3 simultaneously with the thermal insulation measures of the building envelope that must be able to reduce the specific energy / heat use by about 50%. At the same time, it is necessary that the specific emission index for electricity generation be within the limit of I_e<0.150 kg CO_2 / kWh, which leads to national / European efforts to gradually replace traditional electricity generation with those based on renewable energy systems - photovoltaic, *PV* and wind. Romania is in the average area with 0.271 kg CO_2 / kWh compared to the Scandinavian countries emitting below 0.050 kg CO_2 / kWh, and the Central European ones exceeding 0.400 kg CO_2 / kWh, respectively. The efforts of EU countries to replace fossil fuels with renewable energy sources for electricity generation aim for a share of 49% by 2030. At the same time, for the year 2050, an efficiency of the entire process - production,

transport and distribution of electricity is expected to achieve a value of $\eta_{tot}^{2050} = 45\%$, compared to the current value, which is currently about 36% in Romania.

With regard to the operation performance of the heat pump, Annex VII of the RES Directive, Directive 2009/28 / EC requires that "*Only heat pumps for which SPF > 1,15 * 1/η shall be taken into account*", which leads to values of SPF_{HP} >2,56. In addition to this condition, the losses that occur in the operating cycle of the heat pump and which are expressed with the help of COP_{ex} must also be taken into account. As shown by means of the characteristics extracted from data book of an equipment currently existing on the market, the lowest losses correspond to maximal values of the exergetical *COP*. For the analyzed case, maxCOP_{ex} = 0,41 and it occurs at an atmospheric air temperature of approximately T_{air} = +7 ºC and for a water-temperature at the outlet of the heat pump of T_w =37 ºC. But when the atmospheric air-temperature decreases below T_{air} = +7 ºC a higher energy loss appears which is manifested by the decrease of the exergetical *COP*, so that maxCOP_{ex} = 0.29, even in the case of the support provided by an auxiliary electrical resistance.

The increase in energy losses can be seen even at atmospheric air-temperatures exceeding the value of +7 ºC.

It is also important to note that the *relative electrical power* driving the electric motor is adversely affected by atmospheric air-temperatures below +7 ºC, meaning that the price of heat is rising and the associated CO_2 emitted in case of traditional generation of electricity is increased too.

References

1. Proposal for a Directive on energy efficiency (recast), Brussels, 14 July 2021
2. ANNEXES to the COMMISSION RECOMMENDATION Brussels, 25.9.2019 EED Annex IV footnote 4.
3. www.eea.europa.eu/data-and-maps/daviz/co2-emission-intensity Greenhouse gas emission intensity of electricity generation by country. Created 29 Jul 2021. Published 25 Oct 2021. Last modified 25 Oct 2021.
4. Annex VII, DIRECTIVE 2009/28/EC OF THE EUROPEAN PARLIAMENT AND OF THE COUNCIL of 23 April 2009

Light weight gypsum-based material manufactured by expanding process with aluminum powder

Material ușor pe baza de gips fabricat printr-un proces de expandare cu pulbere de aluminiu

Lucian Păunescu[1], Sorin Mircea Axinte[2], Bogdan Valentin Păunescu[3]

[1]Daily Sourcing & Research SRL
95-97 Calea Grivitei street, sector 1, Bucharest 010705, Romania
E-mail: lucianpaunescu16@gmail.com

[2]Department of Applied Chemistry and Materials Science, University „Politehnica" of Bucharest
1-7 Gh. Polizu street, sector 1, Bucharest 011061, Romania
E-mail: sorinaxinte@yahoo.com

[3]Consitrans SA
56 Polona street, sector 1, Bucharest 010504, Romania
E-mail: pnscbogdan@yahoo.com

DOI: 10.37789/rjce.2022.13.2.3

Rezumat. *Lucrarea prezintă metoda de preparare a unui material ușor pe bază de gips. Principiul spumării materiei prime este aplicat la fabricarea betonului aerat autoclavizat prin eliberarea în masa materialului a hidrogenului prin reacția de coroziune a pulberii de aluminiu în soluție apoasă de $Ca(OH)_2$. Originalitatea lucrării este metoda de generare a aluminiului pulbere prin topirea cu microunde a deșeurilor metalice și atomizarea topiturii cu jeturi concentrate de azot. Produsul are densitatea între 530-600 kg/m^3 și rezistența la compresiune între 1,2-2,2 MPa, fiind similar cu betonul aerat autoclavizat, cu domenii de aplicare identice, însă costuri energetice reduse.*

Cuvinte cheie: material ușor, gips, aluminiu, soluție apoasă, microunde, spumare.

Abstract. *The paper presents the preparing method of a light weight gypsum-based material. The raw material foaming principle is applied to the manufacture of aerated autoclavized concrete by hydrogen release in the material mass by the corrosion reaction of aluminum powder in aqueous solution of $Ca(OH)_2$. The work originality is the generation method of powder aluminum by microwave melting of metal waste and melt atomization by concentrated nitrogen jets. The product has density between 530-600 kg/m^3 and compressive strength between 1.2-2.2 MPa, being similar to aerated autoclaved concrete, with identical application fields, but low energy costs.*

Key words: light weight material, gypsum, aluminum, aqueous solution, microwave, foaming.

1. Introduction

In recent decades, the trend of cellular materials made for buildings has intensified. Especially in countries with harsher climates (Sweden, Norway, Finland, Germany, Poland, etc.) this is one of the most effective materials for enveloping the building as panels, small-size blocks and monolithic buildings [1]. Calcined gypsum ($CaSO_4 \cdot 0.5H_2O$) is considered one of the binders with ecological properties suitable for buildings. Despite this quality, its use in this field is quite limited. According to [2], the achievement of light gypsum products with good thermal and acoustic insulation characteristics and lower transport costs could be a solution for the application of gypsum in buildings. A method of reducing the weight of this material is using light inorganic or organic fillers. The best known inorganic fillers are: perlite (an amorphous volcanic glass) and vermiculite (a phyllosilicate mineral). Gypsum products with inorganic fillers available on the market have a bulk density between 300-800 kg/m^3. Limits can be easy exceeded. An experiment presented in [3] shows that 5-10 % perlite added to a mixture of coal fly ash, lime and gypsum, with a low addition of silica fumes, led to a material with the bulk density of 730 kg/m^3 and the compressive strength of 2.3 MPa. The use of vermiculite together with polypropylene fibers has been tested in [4]. The decrease of the product bulk density by about 10 % and the decrease of thermal conductivity by 30 % were obtained with 20 % vermiculite. The negative effect of the test was reducing the mechanical strength by up to 30 %. Fillers of polymeric materials were also tested in gypsum-based materials. Using polystyrene beads (2 %) and polypropylene fiber (2 %), the product bulk density was decreased by half compared to pure gypsum, while the tensile strength increased by 23 % [5]. Other authors have made products with extremely low bulk density (200 kg/m^3), but the mechanical strength has been greatly affected [2, 6]. Natural fillers of vegetable (chopped straw, sawdust, etc.) or animal (chicken feather, cowhide, hoof, etc.) origin were added to the gypsum mass. The paper [7] presents a solution for the use of cork granules with the size below 12 mm. For 20 % cork filler, the product bulk density was around 800 kg/m^3 and very good compressive strength of about 5 MPa was obtained. By addition of 2 % glass fibers, the tensile strength increased nearly 2 times.

Also, obtaining a porous structure either by chemical reactions that release foaming gases for gypsum expansion, or by surface active substances contributes to the decrease of the weight of the gypsum-based material. The best known reaction that releases foaming gas is the reaction of a carbonate (calcium carbonate $CaCO_3$, sodium bicarbonate $NaHCO_3$ or ammonium bicarbonate NH_4HCO_3) with an acidic component (aluminum sulphate $Al_2(SO_4)_3$, sulfuric acid H_2SO_4, boric acid $B(OH)_3$), in which carbon dioxide (CO_2) is released [2]. The most usual foaming method is the release of hydrogen from the reaction of aluminum powder with the aqueous solution of $Ca(OH)_2$, used in the manufacture of aerated autoclaved concrete (AAC). In the first experiments performed with 65 % gypsum, 33 % $Ca(OH)_2$ and 1 % aluminum powder, the bulk density had relatively small values (640 kg/m^3), but the compressive strength was below 1 MPa [8]. Also, the macrostructure of the material was slightly

homogeneous, containing even pores over 5 mm [2]. According to [9], the addition of light fine aggregate (e.g. perlite) homogenizes the macrostructure, and the pore size is significantly reduced.

Several types of waste can be used as substitutes for foaming agents with the ability to release CO_2. Thus, the sludge from the sugar manufacturing process, coal fly ash as a by-product of coal burning in thermal power stations or dust resulting from cutting and polishing marble or granite were used in the manufacturing process of light weight gypsum-based materials such as substituting $CaCO_3$ [2, 10]. According to [10], gypsum based-materials manufactured with dust from stone waste processing had characteristics almost similar to those of aerated autoclaved concrete (bulk density below 600 kg/m^3, thermal conductivity below 0.2 W/m·K and compressive strength around 2 MPa). They are suitable for using as thermal insulation blocks, light weight boards, light weight fire-resistant plasters or thermal insulation plasters.

The objective of the current paper is the manufacture of light weight gypsum-besed material applying an improved technical solution for foaming with aluminum powder aiming to reduce the bulk density and thermal conductivity values and to keep the compressive strength at an acceptable level.

The originality of the work consists on the one hand in applying the own method of producing aluminum powder by spraying the melted aluminum waste with concentrated nitrogen jets in a closed enclosure and on the other hand in adopting new additives compared to the known manufacturing recipes as components of the raw material mixture.

2. Methods and materials

Unlike most processes of foaming silicate raw materials based on chemical reactions to release a gas blocked in the viscous mass (thermally softened) of the mixture, which requires high temperatures (750-1150 ºC) [11], the expansion with hydrogen gas resulting from the corrosion process of aluminum powder in aqueous $Ca(OH)_2$ solution takes place at room temperature. An approximately similar process based on this chemical reaction shown below (1) was successfully tested by the authors' team in a process of foaming the glass waste powder as a raw material mixed with aluminum powder, carboxymethyl cellulose as a stabilizer of the foaming process, $Ca(OH)_2$ and distilled water [12].

$$2Al + 3Ca(OH)_2 + 6H_2O = Ca_3Al_2(OH)_{12} + 3H_2 \quad (1)$$

The cubic $Ca_3Al_2(OH)_{12}$ phase (named katoite) enters in the melting mass of gypsum and the gaseous hydrogen is released. According to the paper [13], the reaction mechanism (1) could include several successive reactions that take place at the separation zone between the outer surface of aluminum particles and the aqueous $Ca(OH)_2$ solution.

$$Al_2O_3 + H_2O = 2AlOOH \quad (2)$$

$$AlOOH + H_2O = Al(OH)_3 \quad (3)$$

$$Al(OH)_3 + OH^- = Al(OH)_4 \quad (4)$$

$$3Ca^{2+} + 2Al(OH)_4 + 3H_2O = Ca_3Al_2(OH)_{12} + 6H_2 \quad (5)$$

The sludge prepared into a ctlindrical metal mold was continously stirred with a metal propeller up to the beginning of expansion process.

The material used in this experiment were: calcined gypsum ($CaSO_4 \cdot 0.5H_2O$), hydrated lime ($Ca(OH)_2$), coal fly ash, perlite, silica fume, carboxymethyl cellulose and aluminum. The oxide composition of coal fly ash, perlite and silica fume are presented in Table 1 [14-16].

Table 1

Oxide composition of coal fly ash, perlite and silica fume

Material	SiO_2 wt. %	Al_2O_3 wt. %	Na_2O wt. %	K_2O wt. %	Fe_2O_3 wt. %	MgO wt. %	CaO wt. %	Other oxides wt. %
Coal fly ash	46.5	23.7	10.1		8.6	3.2	7.9	-
Perlite	70-75	12-15	3-4	3-5	0.5-2	0.2-0.7	0.5-1	-
Silica fume	85-98	< 2.0	< 1.8	< 1.1	< 1.8	< 1.9	< 2.5	< 4.0

Commercially, the calcined gypsum is available ground below 1 mm. Fine grinding and sieving were required for the experimental use, with optimal granulation below 100 μm. The coal fly ash was purchased from the Romanian Paroseni-thermal power station initially with a grain size below 250 μm and after grinding in a ball mill the grain size was reduced to values less than 80 μm. Perlite available on the market is in a granular state being obtained by expanding the ore. Its fine grinding in a ball mill was performed repeatedly until the grain size was reduced below 25 μm, values suitable for its use in the experiment. Silica fume with extremely fineness (below 10 μm) and high silica content was used as such being am effective pozzolanic material, that increases the compressive strength of the material in whose composition it enters. Carboxymethyl cellulose was added in the mixture of solid starting materials as a binder and foam stabilizer. Its solubility in water is very high. For this reason, the fine powder should not be introduced into the water, but the water should be poured over the powder mixture [17].

The aluminum powder with a very fine granulation (below 10 μm) was made by the research team from the Romanian company Daily Sourcing & Research on a molten aluminum waste atomization plant. The waste was melted in a ceramic crucible using an unconventional microwave heating technique and was discharged through a central nozzle. The molten aluminum jet was atomized by the direct contact with several concentrated jets of nitrogen gas distributed at high rate. As a result, a very fine aluminum powder was directed and accumulated to the water-cooled base of the

plant. Figure 1 shows a detail of the atomization area of molten aluminum (a) and a batch of fine aluminum granules (b).

a b

Fig. 1. Details on the atomization of molten aluminum
a – the atomization area of the plant; b – batch of aluminum granules
(Reproduced by permission of Junkoeko SRL Slobozia, Romania).

In principle, the basic manufacturing recipe of gypsum-based material includes gypsum as the main raw material (between 70.7-78.8 %). Coal fly ash (between 3.4-5.1 %), usually a partial replacement of the binder, allowed a slight reduction of the gypsum ratio. Significant proportions of hydrated lime (between 9.5-10.4 %) were adopted to facilitate the corrosion reaction of aluminum in the aqueous solution of $Ca(OH)_2$ and the release of hydrogen as a foaming gas. Silica fume which is an effective pozzolanic material was used in low proportions between 0.7-1.4 %. Perlite with a filler role, which contributes to increasing the bulk density, has been used in a wide range (between 0-10 %). A material that easily forms an aqueous solution and acts as a foam stabilizer was carboxymethyl cellulose used in a low proportion (2 %) kept constant in all four tested variants. Aluminum (3 %) kept constant is the material that practically ensures the foaming process of gypsum by its corrosion reaction in the aqueous medium of $Ca(OH)_2$. The distilled water ratios added supplementary to the mixture of solids varied between 25-35 %.

The proportion of materials used in experiment coresponding to the four variants adopted for manufacturing the gypsum-based materials are presented in Table 2.

Table 2

Weight ratios of materials that compose the experimental variants

Variant	Calcined gypsum wt. %	$Ca(OH)_2$ wt. %	Coal fly ash wt. %	Perlite wt. %	Silica fume wt. %	Carboxy-methyl cellulose wt. %	Aluminum wt. %	Water addition wt. %
1	78.8	10.4	5.1	-	0.7	2.0	3.0	35
2	77.0	10.2	4.8	2	1.0	2.0	3.0	32
3	74.1	10.1	4.6	5	1.2	2.0	3.0	29
4	70.7	9.5	3.4	10	1.4	2.0	3.0	25

Common methods have been applied to characterize the experimentally manufactured gypsum-based materials. The bulk density was determined by the method of dividing the mass of foamed samples loaded into a cylindrical vessel at its volume [18]. To calculate the porosity, the comparison method [19] between the density of the porous sample and the density in compact state (true density) of the same material was applied. Using an analyzer TA.XTplus Texture type, the compressive strength was measured and the Guarded-Comparative-Longitudinal Heat Flow method (ASTM E1225-04) allowed to determine the thermal conductivity value. By the water immersion method (ASTM D570) it was determined the water absorption coefficient of samples. The microstructural characteristics of samples were identified with an ASONA 100X Zoom Smartphone Digital Microscope.

3. Results and discussion

Table 3 presents a synthese of manufacturing process parameters of gypsum-based material. The mass of materials entered in process (dry and wet), the mass of final product, the temperature and duration of foaming process and the index of volume increasing compared to the initial volume are highlighted.

Table 3

Main functional parameters of the expanded process of gypsum

Variant	Dry/wet starting material amount (g)	Process temperature (ºC)	Process duration (min)	Index of volume increasing	Expanded gypsum amount (g)
1	230/310.5	26	11	2.50	218.6
2	230/303.6	26	9	2.20	218.2
3	230/296.7	26	8	2.00	218.9
4	230/287.5	26	6.5	1.70	218.5

The macrostructural apearance of the cross section of samples corresponding to the four experimental variants is shown in Figure 2.

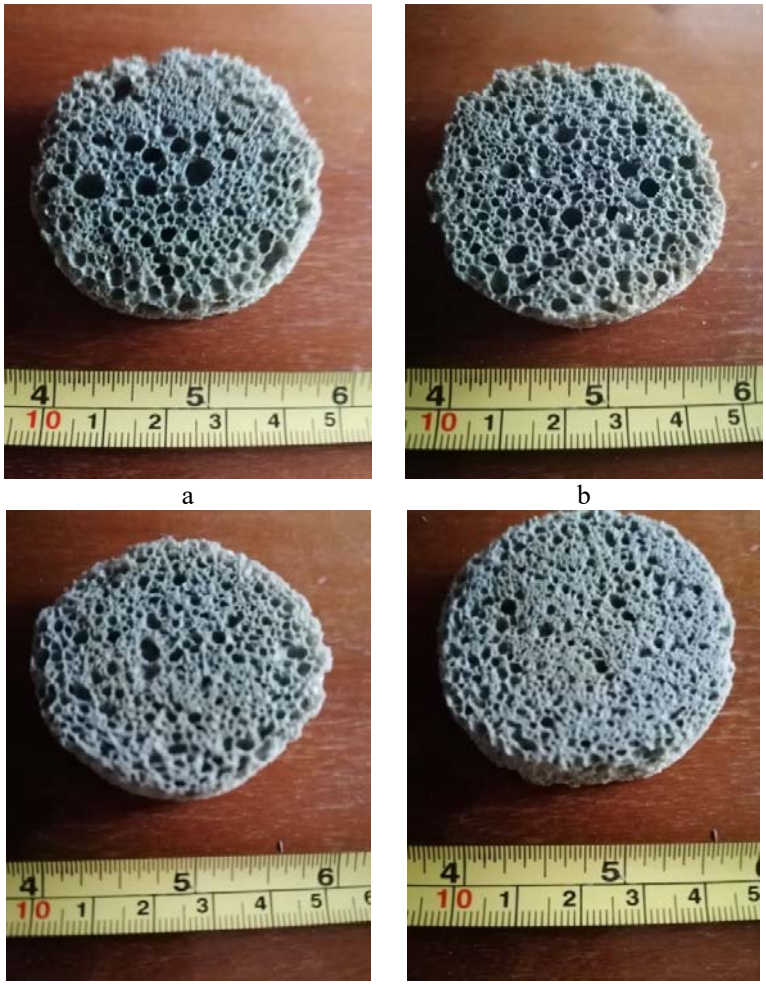

a b c d

Fig. 2. Macrostructural apprearance of the cross section of samples
a – variant 1; b – variant 2; c – variant 3; d – variant 4.

According to the data in Table 3, the dry starting material was estabilished at 230 g and, due to the variation of water addition proportion, its wet mass was between 287.5-310.5 g. The ambient temperature at which the manufacturing process took place was 26 ºC kept constant during the experiment. The foaming process was completed in a variable time period between 6.5-11 min, the increase in volume of the starting material being 2.50 in the case of variant 1 and only 1.70 in the case of variant 4. Examining the pictures in Figure 2, the change of the macrostructural appearance of the samples can be observed. If in the case of variant 1 the structural inhomogeneity is characteristic, in the case of variant 4 its macrostructure is significantly improved. The improvement of this property has an increasing trend from variant 1 to variant 4. Practically, the highest coal fly ash proportion (5.1 %), the lowest silica fume proportion (0.7 %) and the total absence of perlite were the decisive factors that determined the maximum expansion of gypsum-based material in variant 1. In

contrast, the reduction of coal fly ash to 3.4 %, the increase of silica fume to 1.4 % and the large increase in perlite up to 10 % created an obviously denser product with much improved macrostructural homogeneity by decreasing the pore size and uniformizing their distribution (variant 4). The main physical, thermal, mechanical and microstructural characteristics of the gypsum-based material samples are presented in Table 4.

Table 4

Main physical, thermal, mechanical and microstructural characteristics of samples

Variant	Bulk density (kg/m^3)	Porosity (%)	Thermal conductivity (W/m·K)	Compressive strength (MPa)	Water absorption (vol. %)	Pore size (mm)
1	530	74.7	0.177	1.2	3.7	0.4-4.5
2	552	73.7	0.161	1.6	3.5	0.7-2.6
3	586	72.1	0.129	1.9	3.7	0.6-2.2
4	600	71.4	0.184	2.2	3.9	0.4-0.8

The main objective of the experiment was to manufacture a light weight gypsum-based material with a relatively low bulk density for this material type. From the data of Table 4, a range of this physical feature values between 530-600 kg/m^3 represents the achievement of the objective. The material porosity had normal values between 71.4-74.7 %. The structural inhomogeneity of the samples made in variants 1 and 2 had a negative influence on the thermal conductivity, which at the low density values should have reached its lowest values. However, the thermal conductivity of variants 1 and 2 was higher than theoretically (0.177 and 0.161 W/m·K, respectively). According to the authors' forecast, the compressive strength of variant 4 (the densest from a structural point of view) had a maximum value (2.2 MPa), the other variants following a decreasing trend up to variant 1 (1.2 MPa). The water absorption was identified to be within a normal range (between 3.5-3.9 vol. %). The characteristics of gypsum-based material are close to the characteristics of aerated autoclaved concrete (AAC) [20], as also observed by the authors [2], this material being suitable for light weight boards and blocks, fire-resistant plasters and thermal insulation plasters. The investigation of the microstructural characteristics of the samples was performed based on the images presented in Figure 3.

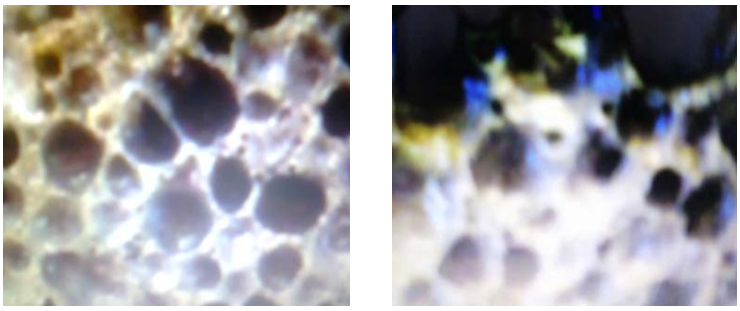

a b

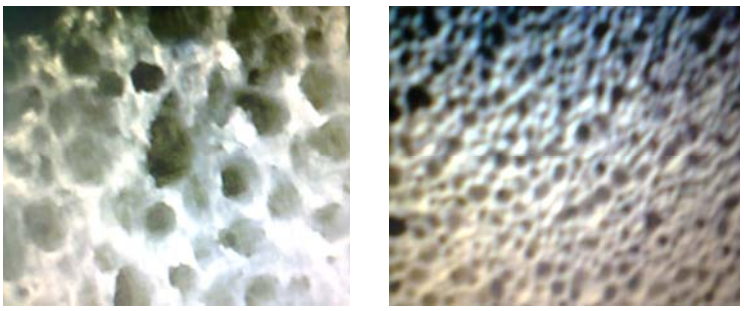

Fig. 3. Microstructural characteristics of the gypsum-based material samples
a – variant 1; b – variant 2; c – variant 3; d – variant 4.

The images in Figure 3 allowed to determine the pore size of the four analyzed samples. The results, also included in Table 4, are: 0.4-4.5 mm (variant 1), 0.7-2.6 mm (variant 2), 0.6-2.2 mm (variant 3) and 0.4-0.8 mm (variant 4). Obviously, the most homogeneous pore distribution belongs to variant 4 and the most inhomogeneous belongs to variant 1.

The aerated autoclaved concrete (AAC) considered as a reference for the gypsum-based material is a light weight concrete type, which does not contain aggregates like conventional concretes. It consists of sand (as a supplier of silica) and coal fly ash as raw materials and aluminum powder as a hydrogen supplier for foaming. Despite the energy consumption in autoclave, the total energy used in the manufacturing process is 50% lower than the energy consumption of Portland cement production [20] required in the common concrete. So, like AAC, the gypsum-based material is an energy-efficient product. Unlike the conventional concrete, AAC can't be used as a finish. Being much more porous (pore size between 50-500 μm, compared to a maximum of 5 μm in conventional concrete), an exterior cladding is required, so that the moisture is not absorbed. The method of producing fine aluminum powder adopted by the authors in the current work by microwave melting of aluminum waste with nitrogen is also an energy-efficient method.

4. Conclusions

A light weight material, whose use in building construction is similar to that of aerated autoclaved concrete, but whose cumulative energy consumption is significantly lower, was experimentally small scale-manufactured in the Romanian company Daily Sourcing & Research. This material, based on gypsum, was performed of calcined gypsum ($CaSO_4 \cdot 0.5H_2O$) available on the market, finely ground (above 70 %) together with coal fly ash (3.4-5.1 %), an industrial by-product of thermal power stations. The raw material expansion occurs at the ambient temperature and is based on the corrosion reaction of a fine powder aluminum in aqueous solution of $Ca(OH)_2$, that releases hydrogen gas. The hydrogen forms bubbles with controllable size through the perlite addition (up to 10 %). The aqueous solution of carboxymethyl cellulose (2 %) acts as a foam stabilizer. The gypsum-based material produced in this experiment had

the following characteristics: Bulk density between 530-600 kg/m^3, porosity between 71.4-74.7 %, thermal conductivity in the range 0.129-0.184 W/m·K, compressive strength between 1.2-2.2 MPa and water absorption below 3.9 vol. %. The pore size had the lowest values (between 0.4-0.8 mm) in the case of variant 4 (with the highest perlite addition of 10 %) and reached the highest values (up to 4.5 mm) in the case of variant 1 (without perlite addition). The originality of the paper is mainly applying the own technique of preparing aluminum powder by spraying the melted aluminum waste with concentrated nitrogen jets in a closed enclosure and also in adopting new additives in the manufacturing recipe of the final product.

5. Acknowledgement

The paper used for the experiment to make materials manufactured and tested experimentally in the Project co-financed by the European Regional Development Fund through the Competitiveness Operational Program 2014-2020 ECOWAVNEFDE (financing contract no. 22 from 04.10.2017) having as beneficiary JUNKOEKO SRL Slobozia, Romania.

References

[1] L.V. Il'ina, M.A. Rakov, „Non-Autoclaved Aerated Concrete With Mineral Additives", AIP (American Institute of Physics) Proceedings, vol. 1698, 070007 pp. 1-5, 2016. https://www.doi.org/10.1063/1.4937877

[2] Magdalena Doleželová, Jitka Krejsová, Alena Vimmrová, „Lightweight Gypsum Based Materials: Methods of Preparation and Utilization", International Journal Sustainable Development Planning, vol. 12, no. 2, 2017, pp. 326-335, Proceedings of the 6th International Conference on Harmonisation between Architecture and Nature (Eco-Architecture 2016), Alicante, Spain, July 13-15, 2016.

[3] I. Demir, M. Baspinar Serhat, „Effect of Silica Fume and Expanded Perlite Addition on the Technical Properties of the Fly Ash-Lime-gypsum Mixture", Construction and Building Materials, vol. 22, no. 6, 2008, pp. 1299-1304. http://dx.doi.org/10.1016/j.conbuildmat.2007.01.011

[4] O. Gencel, J.J. del Coz Diaz, M. Sutcu, „Properties of Gipsum Composites Containing Vermiculite and Polypropylene Fibers: Numerical and experimental results", Energy and Buildings, vol. 70, 2014, pp. 135-144. http://dx.doi.org/10.1016/j.enbuid.2013.11.047

[5] B. Sayil, E. Gurdal, „The Physical Properties of Polystyrene Aggregated Gypsum Blocks", Proceedings of the 8th International Conference on Durability Materials and Components, Vancouver, Canada, May 30-June 3, 1999, vol. 1-4, pp. 496-504.

[6] A.F.J. Gonzáles Madariaga, J. Lloveras Macia, „Mezclas de Residous de Poliestireno Expandido (EPS) Conglomerados con Yeso o Escayola para su Uso en la Construcción", Informes de la Construcción, vol. 60, no. 509, 2008, pp. 35-43.

[7] F. Hernandez-Olivarez, M.R. Bollati, M. Del Rio, B. Parga-Landa, „Development of cork-gypsum composites for building applications", Construction and Building Materials, vol. 13, no. 4, 1999, pp. 179-186. http://dx.doi.org/10.1016/S0950-0618(99)00021-5

[8] Alena Vimmrová, M. Nazmunnahar, R. Černý, „Lightweight Gypsum-Based Materials Prepared with Aluminum Powder as Foaming Agent", Cement Wapno Beton, vol. 19, no. 5, 2014, pp. 299-307.

[9] Alena Vimmrová, M. Keppert, L. Svoboda, C. Robert, „Lightweight Gypsum Composites: Desigh Strategies for Multi- Functionality", Cement & Concrete Composites, vol. 33, no. 1, 2011, pp. 24-89.
[10] Jitka Krejsová, Renata Schneiderová Heralová, Magdalena Doleželová, Alena Vimmrová, „Environmentally Friendly Lightweight Gypsum-Based Materials with Waste Stone Dust", Proceedings of the Institution of Mechanical Engineers, Part L: Journal of Materials: Desigh and Applications, vol. 233, no. 3, 2019.
[11] G. Scarinci, G. Brusatin, E. Bernardo, „Glass Foams" in Cellular Ceramics: Structure, Manufacturing, Properties and Applications, Wiley-VCH GmbH & KgaA, M. Scheffler, P. Colombo eds., Weinheim, Germania, 2005, pp. 158-176.
[12] L. Paunescu, S.M. Axinte, B.V. Paunescu, „New Manufacturing Method of Glass Foam by Cold Expansion of Glass Waste", Journal La Multiapp, vol. 2, no. 3, 2021, pp. 1-9.
[13] S. Kaneshira, S. Kanamori, K. Nagashima, T. Saeki, H. Visbal, T. Fukui, K. Hirao, „Controllable Hydrogen Release Via Aluminium Powder Corrosion in Calcium Hydroxide Solution", Asian Ceramic Societies, vol. 1, vol. 3, 2013, pp. 296-303.
[14] M.F. Dragoescu, L. Paunescu, „Nonconventional Heating Method Used to Obtain Glass Foam from Clear Flat Glass Waste", Nonconventional Technologies Review, vol. 22, no. 2, 2018, pp. 36-40.
[15] Mueena Samar, Shweta Saxena, „Study of Chemical and Physical Properties of Perlite and its Application in India", International Journal of Science Technology and Management, vol. 5, no. 4, 2016, pp. 70-80.
[16] *** „About Silica Fume", European Silica Fume Committee, 2021. https://www.microsilicatefume.eu/page/composition_silica_fume_amorphous_silicon_dioxide/f1.html
[17] R. Ergun, J. Guo, B. Huebner-Keese, „Cellulose-Carboxymethyl Cellulose", Encyclopedia of Food and Health, 2016, pp. 694-702. https://www.doi.org/10.1016/B978-0-12-384947-2.00127-6
[18] *** „Aggregates for Concrete" (Chapter 5) in Design and Control of Concrete Mixtures, 16 edition (2016), Portland Cement Association Publishing, Skokie, Illinois, US. http://www.ce.memphis.edu/1101/notes/concrete/PCA_manual/Chap05.pdf
[19] L.M. Anovitz, D.R. Cole, „Characterization and Analysis of Porosity and Pore Structures", Reviews in Mineralogy and Geochemistry, vol. 80, 2005, pp. 61-164.
[20] N. Narayanan, K., K. Ramamurthy, „Structure and Properties of Aerated Concrete: A review", Cement & Concrete Composites, vol. 22, 2000, pp. 321-329.

Biofilters efficiency in removing ammonium from water intended for human consumption

Eficiența biofiltrelor în eliminarea amoniului din apa destinată consumului uman

G Radu, G Racoviteanu, E Vulpasu

Technical University of Civil Engineering Bucharest, Romania
Blvd Lacul Tei 124
Email: *gheorghe.radu23@gmail.com*

DOI: 10.37789/rjce.2022.13.2.4

Abstract. Nitrogen is the most abundant element of Earth atmosphere and is a component part of all living organism, being found in DNA and RNA. In most ecosystems, ammonium is the main source of nitrogen for plants. In natural water sources, ammonium concentrations are usually low, but due to industrial, agricultural and other human activities, its concentration is quite high. In water supply systems it leads to degradation of water quality and to formation of other by-products with effects on human health. Existing technologies used to reduce the ammonium concentration in water are ion exchangers, biological filtration, air stripping, breakpoint chlorination and reverse osmosis. This article is based on experimental tests aimed to determine the efficiency of biofilters in reducing the ammonium concentrations in water, depending on the carrier/filtration media used in the biofilters, depending on the ammonium concentration in raw water and depending the contact time between water and the attached biomass, but also the impact of the sudden change of ammonium concentration in the raw water on the biofilters efficiency.

Key words: nitrogen, biofilters

1. General data

Nitrogen is an essential nutrient for plants and animals [1]. In nature, nitrogen is found in many forms, and its transformation from one form to another is described by the nitrogen cycle. The atmosphere is made up of 79% nitrogen gas. Although the atmosphere is practically an inexhaustible reservoir of nitrogen gas, nitrogen must be first combined with hydrogen or oxygen in order to be assimilated by plants and then to be consumed by animals [2].

In living organisms, nitrogen is found in amino acids, in proteins, in nucleic acids (DNA and RNA) and in the energy transfer molecule, adenosine triphosphate. The human body contains 3% nitrogen by mass.

Ammonia is a colorless gas, which has a pungent odor at room temperature and which under pressure can become liquid. Ammonia dissolves easily in water, in which

most of the ammonia (depending on temperature, pH and amount of dissolved matter) is converted to ammonium cations by protonation. In water, a balance is established between dissolved ammonia and ammonium [3].

Ammonium and nitrate are the primary sources of nitrogen for plants, but the assimilation of ammonium requires less energy than the assimilation of nitrate and for this reason ammonium is the first element absorbed when plants are nitrogen deficient. However, large amounts of ammonium can be toxic, so the absorption of ammonium must be controlled to avoid its toxicity to plants [4].

Ammonium itself has no toxic effects on the human or animal health and would not limit the use of water, its sanitary importance consists in the fact that it indicates the pollution of water with other chemical or especially bacteriological elements that can have harmful effects on human health [3] [5].

Ammonium concentrations in non-degraded natural water sources are usually low, but ammonium concentrations from intensive agriculture, industrial and other human activities have a negative impact on water sources.

In particular, in the case of surface water sources, the presence of ammonium in very high concentrations decreases the dissolved oxygen concentration and leads to toxicity of the aquatic environment, increased corrosion rate in the soil, algae development and finally leads to eutrophication of lakes. Eutrophication is a global problem and has been identified as a major problem for water source management [6].

In the drinking water treatment plants, the excess concentrations of ammonium are undesirable because the presence of excess ammonium in water leads to an increase in the consumption of chlorine used in disinfection and thus to a reduction of the efficiency in the disinfection stage of the treatment plant. Ammonium can interfere with manganese removal filters, as oxygen would be used largely for ammonium nitrification, resulting in an earthy taste [7].

Its presence in the distribution networks leads to the development of bacteria on the pipes walls of which the distribution network is composed and to the oxidation of ammonium to nitrites and nitrates.

Nitrites and nitrates formed by oxidative conditions in distribution networks are toxic compounds that lead to the oxidation of divalent iron from hemoglobin to trivalent iron, preventing the transport of oxygen to tissues and leading to methemoglobinemia, especially at infants [3] [8].

Ammonium leads to the degradation of water quality by changing its taste and smell, which can create problems of water acceptability to consumers [3].

In Romania, the maximum allowed concentration for ammonium in drinking water, according to Law 458/2002 is 0.50 mg/l. Also, the 2184 /2020/EU Directive impose a maximum concentration of 0.5 mg/l for ammonium [9][10].

Over time, several methods have been developed to reduce the ammonium concentration in water, namely: physical, chemical, biological methods or a combination of these methods. These mainly include: ion exchangers, biological filtration, air stripping, breakpoint chlorination and reverse osmosis [11].

Nitrification is the biological process of ammonium oxidation to nitrate with the intermediate form nitrite. Nitrification is performed by species of bacteria called

Nitrosomonas and Nitrobacter [12]. These two species of bacteria are distinguished from each other by the ability to oxidize only certain nitrogen compounds. Nitrosomonas oxidizes ammonium to nitrite and Nitrobacter oxidizes nitrite to nitrate. Both species of bacteria are classified as autotrophic organisms (they do not need a source of organic carbon, they use carbon dioxide for synthesis) [13] [14] [15].

The stoichiometric equations of nitrification for Nitrosomonas and Nitrobacter are [11]:

$$NH_4^+ + 1.5\ O_2 \rightarrow 2H^+ + H_2O + NO_2^- \text{ (Nitrosomonas)} \quad (1)$$

$$NO_2^+ + 0.5\ O_2 \rightarrow NO_3^- \text{ (Nitrobacter)} \quad (2)$$

$$NH_4^+ + 2\ O_2 \rightarrow NO_3^- + 2H^+ + H_2O \quad (3)$$

The above equation represents the compound equation of ammonium oxidation to nitrate made by Nitrosomonas and Nitrobacter.

Nitrification process is influenced by certain factors such as temperature, dissolved oxygen concentration, pH and inhibitor concentration [13] [14].

The biological processes used to reduce ammonium in water for human consumption are mainly processes with biomass attached. Biofilters are characterized by the presence of microorganisms that adhere to the filtration media in the form of a fixed film (biofilm) [16].

For any filtration media used, all biofilters follow the same principle, namely: biological degradation of pollutants by microorganisms fixed on the filtration media surface.

2. Materials and Methods

2.1. Purpose of experimental tests

In order to reduce the ammonium concentration in water, in the performed experimental tests, it was proposed and used a biological processes with attached biomass.

The main purpose of the experimental tests was to determine the efficiency of biofilters for reducing ammonium concentrations in water, depending on the filtration media used in the biofilter, on the ammonium concentration in the raw water and on the contact time between water and attached biomass. In addition to this main purpose, the experimental tests aimed to determine the impact of sudden change of the ammonium concentration in raw water on the biofilter efficiency in reducing its concentration in water, compared to the biofilter efficiency obtained after a period of one week in which synthetic raw water with the same ammonium concentration was introduced into the biofilters.

2.2. Experimental stand

The experimental tests were performed at laboratory level on an experimental stand that is part of the Colentina Laboratory Complex, a complex belonging to the Technical University of Civil Engineering of Bucharest.

The experimental stand is represented by a pilot installation, consisting of 3 biofilters with fixed bed and ascending flow.

The following figure shows the technological scheme of the experimental stand of biofilters and its component objects.

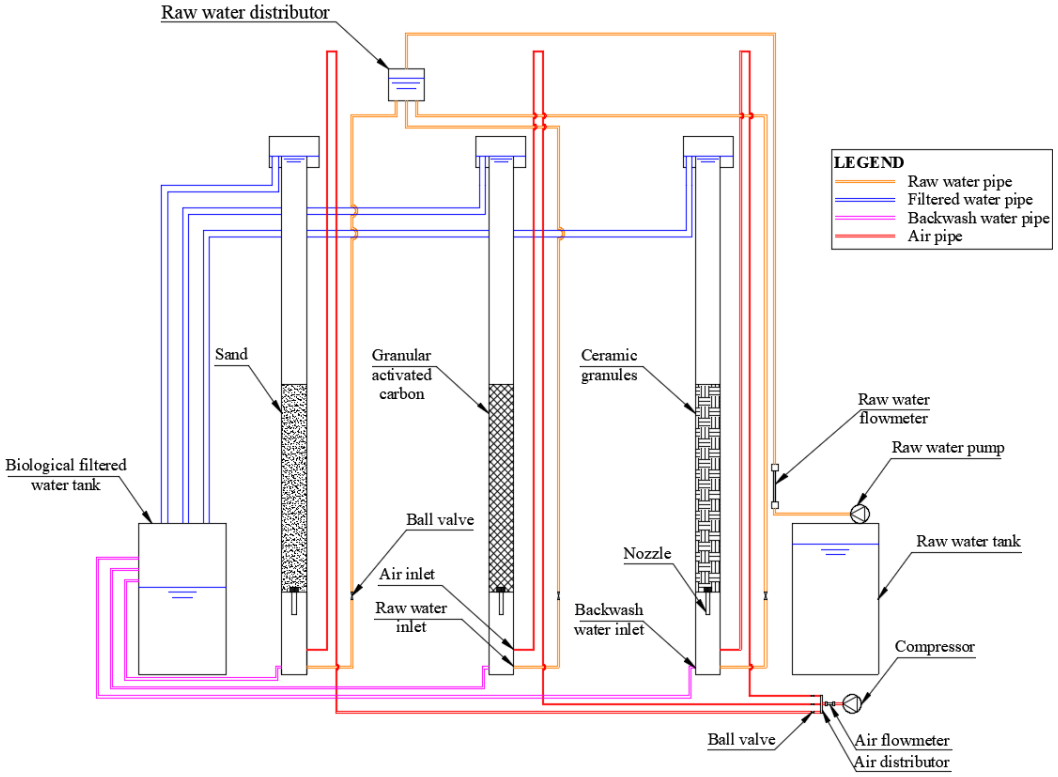

Figure 1. Technological scheme of biological filtration installation and component objects.

Considering that the experimental stand consists of 3 biofilters and because 3 filtration media were available, in the experimental tests, in each biofilter only one type of filtration media was used. The filtration media used and analyzed in the experimental tests are: sand, ceramic granules and granular activated carbon. These are shown in the following figure.

Figure 2. Filtration media.

2.3. Raw water

2.3.1. Raw water from well. The experimental stand is based on biological processes with biomass attached, and to help the start of the biological process and maintain its stability until the end of experimental tests, it was decided to use untreated water with bacteriological development potential.

The raw water used in the experimental tests comes from a well near Bucharest.

The following table presents the quality parameters of the raw water from the well and used in the experimental tests.

Table 1. Raw well water quality parameters.

Nr.	Water quality parameter	Minimum values	Average values	Maximum values
1	Ammonium [mg/l]	0.17	0.63	1.12
2	Nitrates [mg/l]	91.80	146.40	230.10
3	Nitrites[mg/l]	0.040	0.285	0.575
4	Phosphorus [mg/l]	0.029	0.032	0.036
5	pH	6.71	7.78	8.24
6	Conductivity [µS/cm]	845.00	1089.38	1327.00

2.3.2. Syntetic raw water In order to increase and vary the ammonium concentration in the raw water, up to the ammonium concentration necessary to perform the test, synthetic raw water was prepared by adding ammonium chloride NH_4Cl in the raw water from the well.

To obtain the desired ammonium concentration in raw water, has been calculated the required dose of ammonium chloride to be added in water.

2.4. Water parameters

To determine the raw water and biologically filtered water quality parameters, the existing glassware and equipments of the Colentina laboratory was used.

Ammonium, nitrates, nitrites and phosphorus concentrations were determined with the Hach spectrophotometer DR3900, using the reagents and methods of determination specified in the spectrophotometer user manual.

Determinations of pH, conductivity, temperature and dissolved oxygen was performed using a multimeter with two channels Hach HQ440D and a pH-meter Marvel pH526, using the provided sensors.

2.5. Initiation of the biological process

Unlike other existing technologies for reducing the ammonium concentration in water, biofilters cannot be used immediately, and require a period of priming of the biological process. In order to perform the experimental tests, a period of the biological process priming was needed, respectively a period for Nitrosomonas and Nitrobacter growth.

According to the analyzes performed, after the water was transported 3-4 times per week constantly, without even a week of interruption due to traffic restrictions generated by SARS-COV 2 virus, after about a month later, the biological process was primed.

2.6. Experimental tests

In the experimental tests were proposed and performed 3 test phases, in which the efficiency of biofilters in reducing the ammonium concentration in water was analyzed.

The tests performed in phases I and II, aimed to evaluate the efficiency of the biological process on each filtration media, depending on the ammonium concentration in raw water and depending on the contact time between water and biomass. The tests performed in phase III aimed to increase the efficiency of the biological process in reducing the ammonium concentration in raw water by evaluating the influence of external sources of nutrients in case of their addition to water.

The following table shows the raw water flows and ammonium concentrations in experimental tests.

Table 2. Experimental phases

Phase	Test	$Q_{raw\ water}$ [l/h]	$Q_{raw\ water/filter}$ [l/h]	$C_{ammonium}$ [mg/l]	Remarks
I	1	60	20	≅2	Without nutrients
	2	60	20	≅5	
	3	60	20	≅10	
II	1	105	35	≅2	
	2	105	35	≅5	
	3	105	35	≅10	
III	1	60	20	≅5	With nutrients

Even if the amount of ammonium chloride added into the water was calculated to obtain the desired concentration, in reality the concentrations obtained were approximately equal to those desired. The names used for ammonium concentrations in this article are:

- low concentrations: 0.5-4 mg/l;
- average concentrations: 4-8 mg/l;
- high concentrations: 8-12 mg/l.

3. Results and Discutions

The pilot plant was monitored by measurements of factors influencing the biological process, such as temperature, pH and dissolved oxygen.

The nitrification process takes place at temperatures between 4 and 45°C, with an optimal temperature of 35°C for Nitrosomonas and an optimal temperature of 35-42°C for Nitrobacter [14].

For an optimal functioning of the nitrification process, it is recommended that the minimum level of dissolved oxygen concentration be 2 mg/l [14].

For the operation of the nitrification process, it is recommended that the pH be maintained in the range of 6.5-8, with an optimal pH of 7.2 [14].

3.1. Biofilter's efficiency in phase I

The first phase consisted of 3 tests, in which, in each biofilter, raw water was introduced with a flow rate of 20 l/h and with 3 different ammonium concentration (one concentration for each test).

The following table presents the results of experimental tests obtained for biologically filtered water on the three biofilters in phase I, after normal operation for one week with approximately constant ammonium concentration in raw water.

Table 3. Raw water and biologically filtered water quality parameters in phase I - operation for one week with approximately equal ammonium concentration in raw water

Item	Water sample	NH_4^+ [mg/l]	Efficiency [%]	P [mg/l]	NO_3^- [mg/l]	NO_2^- [mg/l]	PH	Cond. [µS/cm]	DO[e] [mg/l]	T [°C]
$C_{1\text{-}NH_4^+}$= 1.76 mg/l										
1	SRW[a]	1.76	-	0.032	91.8	0.08	6.71	945	7.31	23.3
2	BFWS[b]	0.38	78%	0.029	95.3	0.049	7.68	933	5.11	24.3
3	BFWCG[c]	0.24	86%	0.028	96.1	0.05	7.51	871	5.12	24.1
4	BFWAC[d]	0.59	66%	0.028	95.1	0.044	7.56	965	4.81	24.3
$C_{2\text{-}NH_4^+}$= 4.68 mg/l										
5	SRW[a]	4.68	-	0.032	163.3	0.204	7.82	1004	6.88	22.8
6	BFWS[b]	0.69	85%	0.028	173.9	0.41	7.21	936	4.74	23.4
7	BFWCG[c]	0.51	89%	0.026	175.0	0.522	7.46	937	4.74	23.3
8	BFWAC[d]	0.95	80%	0.027	174.3	0.486	7.27	1004	4.64	23.2
$C_{3\text{-}NH_4^+}$=10.69 mg/l										
9	SRW[a]	10.69	-	0.03	230.1	0.575	8.24	1232	7.00	22.1
10	BFWS[b]	3.79	65%	0.022	251.5	0.581	8.25	1158	5.14	22.4
11	BFWCG[c]	0.56	95%	0.024	262.7	0.586	8.06	1168	4.95	22.5
12	BFWAC[d]	2.9	73%	0.025	255.1	0.583	8.06	1186	4.70	22.4

[a] Synthetic raw water.
[b] Biologically filtered water on sand.
[c] Biologically filtered water on ceramic granules.
[d] Biologically filtered water on granular activated carbon.
[e] Dissolved oxygen.

Analyzing the results obtained for ammonium and nitrates, it can be seen that the ammonium concentration in biologically filtered water decreases and the concentration of nitrates increases, resulting that the biological nitrification process works, ammonium being oxidized to nitrate.

The following figure shows the efficiencies obtained on each biofilter in phase I in order to reduce the ammonium concentration in the water, when installation was operated for one week with approximately equal ammonium concentration in water.

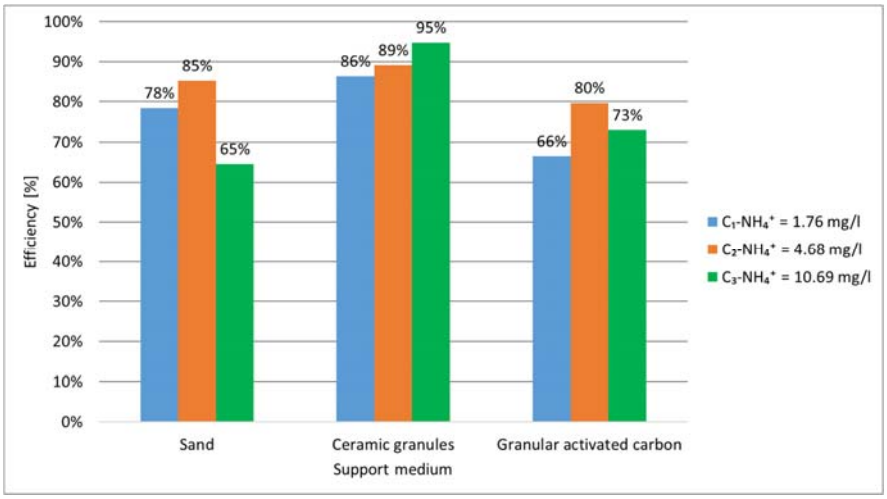

Figure 3. Biofilter efficiency of reducing the ammonium concentration depending on the filtration media used and the ammonium concentration in the raw water introduced in the biofilters - phase I.

As it can be seen in the figure above, in phase I, for any ammonium concentration in raw water introduced in biofilters, the highest efficiencies for ammonium concentration reduction was obtained for the biofilter having ceramic granules as filtration media. For this biofilter, it is observed that if ammonium concentration in the raw water is higher, the efficiency of the biofilter in reducing ammonium increases.

The biofilter that uses sand as filtration media, has higher efficiencies in reducing ammonium at low and medium concentrations, compared to the biofilter with granular activated carbon. At high concentrations, the granular activated carbon biofilter is more efficient than the sand biofilter.

For both, sand biofilter and the granular activated carbon biofilter, the best efficiency is obtained at average ammonium concentrations in raw water.

3.2. Biofilter's efficiency in phase II

The second phase consisted of 3 tests, in which, in each biofilter, raw water was introduced with a flow rate of 35 l/h and with 3 different ammonium concentration (one concentration for each test).

The following table shows the results of experimental tests obtained for biologically filtered water on the three biofilters in phase II, after normal operation for one week with approximately constant ammonium concentration in water.

Table 4. Raw water and biologically filtered water quality parameters in phase II - operation for one week with approximately equal ammonium concentration in raw water

Item	Water sample	NH_4^+ [mg/l]	Efficiency [%]	P [mg/l]	NO_3^- [mg/l]	NO_2^- [mg/l]	PH	Cond. [µS/cm]	DO [mg/l]	T [°C]
$C_{1\text{-}NH_4^+}$=2.81 mg/l										
1	SRW[a]	2.81	-	0.035	145.2	0.04	7.76	1321	7.70	22.1
2	BFWS[b]	1.39	51%	0.027	149.3	0.18	7.95	1196	5.45	22.1
3	BFWCG[c]	0.62	78%	0.029	150.7	0.08	8.09	1137	5.35	22.2
4	BFWAC[d]	0.77	73%	0.028	149.9	0.038	8.04	1139	5.40	22.1
$C_{2\text{-}NH_4^+}$=5.15 mg/l										
5	SRW[a]	5.15	-	0.032	99.6	0.261	8.08	890	7.23	23.7
6	BFWS[b]	3.41	34%	0.028	104.4	0.374	8.11	845	4.83	23.5
7	BFWCG[c]	1.83	64%	0.026	108.2	0.555	8.15	815	5.00	23.7
8	BFWAC[d]	1.87	64%	0.027	109.0	0.144	8.19	879	4.56	23.9
$C_{3\text{-}NH_4^+}$=11.03 mg/l										
9	SRW[a]	11.03	-	0.029	148.4	0.551	8.11	845	7.16	24.6
10	BFWS[b]	6.59	40%	0.027	161.5	0.58	8.05	851	4.86	24.7
11	BFWCG[c]	1.94	82%	0.027	176.7	0.586	7.7	858	4.76	24.6
12	BFWAC[d]	4.97	55%	0.03	167.2	0.582	7.98	861	4.58	24.9

Similar to phase 1, the nitrate concentration increases and the ammonium concentration decreases, resulting that the biological nitrification process works, ammonium being oxidized to nitrate.

The following figure shows the efficiencies obtained on each biofilter in phase II in order to reduce the ammonium concentration in water, when installation was operated for one week with approximately equal ammonium concentration in water.

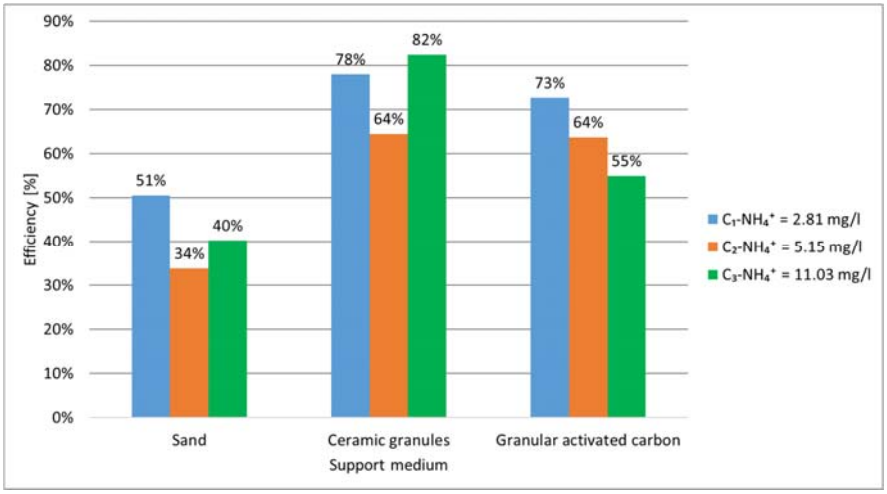

Figure 4. Biofilter efficiency of reducing the ammonium concentration depending on the filtration media used and the ammonium concentration in the raw water introduced in the biofilters - phase II.

As it can be seen in the figure above, in phase II, for any ammonium concentration in raw water introduced in biofilters, the highest efficiencies in reducing

ammonium were obtained for the biofilter having as filtration media ceramic granules, followed by the biofilter with granular activated carbon and sand biofilter. For this biofilter with ceramic granules, it is observed that in case of high concentrations of ammonium, the best efficiency in reducing ammonium in water was obtained, followed by efficiency for low concentrations and efficiency for average concentrations.

The biofilter that uses sand as a filtration media, has the lowest efficiencies in reducing ammonium it is observed that if the concentration increases, the efficiency of this biofilter decreases.

In the case of the biofilter that has granular activated carbon as filtration media, it is observed that if ammonium concentration in the raw water is higher, the efficiency of the biofilter in reducing the ammonium decreases.

As it can be seen in the previous table, a reduction of the contact time between water and the attached biomass, by introducing a higher flow through the installation, the efficiency decreases for all biofilters, but the least affected is the biofilter with ceramic granules, being also the most efficient biofilter in reducing the ammonium concentration at low or high contact time.

For both phases, in case of sudden change of ammonium concentration in raw water for example from 5 mg/l to 10 mg/l there was a small decrease in the efficiency of biofilters, but the most relevant results are those at the end of the week, after normal operation of biofilters.

3.3. Biofilter's efficiency in phase III

In the tests performed in phases I and II, approximately 95% efficiencies were obtained in the reduction of ammonium concentration for the biological filter with ceramic granules, but for any ammonium concentration in the raw water, after biological filtration, the ammonium concentration does not fall below the minimum value of 0.24 mg/l.

In the first phases it was also observed that the concentration of phosphorus in water is very low, phosphorus being a necessary nutrient in the nitrification process. For this reason, in this phase, a new test was performed, with the addition of phosphoric acid (0.26 mg/l) in the synthetic raw water, to check if a better efficiency in reducing ammonium is obtained.

In order to be able to compare the results obtained with the previous tests, the same water flow (20 l/h on each filter) was used and a concentration approximately equal to 5 mg/l, respectively the raw water flow and the ammonium concentration in the water, were approximately equal to those in test 2, from phase I.

The following figure shows the efficiencies obtained for biological filtration in phase III.

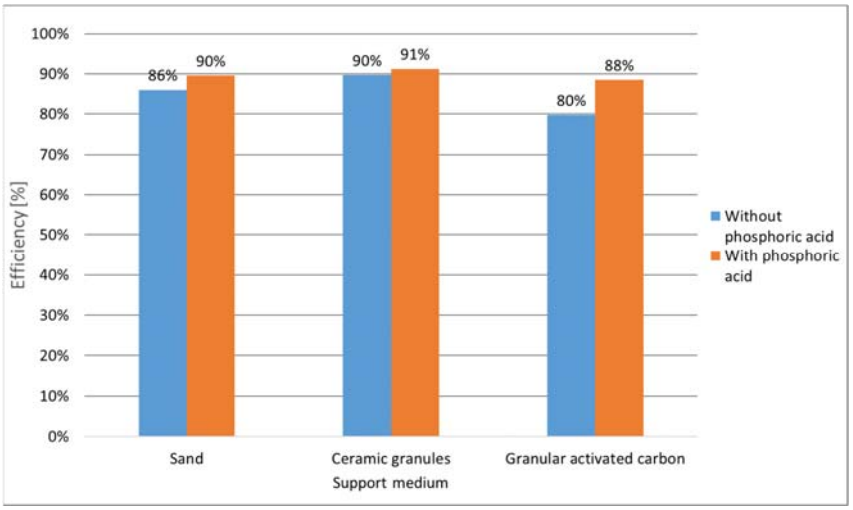

Figure 5. Biofilters efficiency of reducing the ammonium concentration depending on the filtration media used - phase III.

Comparing the results obtained regarding the efficiencies of the biological process in reducing ammonium for normal operation and operation with the addition of phosphoric acid, it is observed that similar efficiencies are obtained in both cases, with one small exception, a small increase in ammonium concentration reduction efficiency for raw water with phosphoric acid.

4. Conclusions

According to the results obtained from the experimental tests, the following can be stated:

- The biological nitrification process worked during the experimental tests, considering that a reduction of ammonium concentration was obtained simultaneously with an increase of nitrate concentration in treated water, indicating oxidation of ammonium to nitrate;
- The results obtained after the operation of the installation for a week with an approximately constant ammonium concentration in the synthetic raw water, indicate that in all tests in the three phases, the biofilters that use ceramic as a filtration media have the highest efficiency (over 64%) in reducing ammonium, for all ammonium concentration in the raw water introduced into the biofilters;
- The biological process is affected by the contact time reduction between water and the attached biomass, because according to the results, the efficiencies of all biofilters decreased as the contact time decreased. However, the biofilter with ceramic granules was the least affected by the reduction of the contact time, being the most efficient biofilter in reducing the concentration of ammonium in the raw water in all the analyzed cases.
- In case of sudden change of ammonium concentration in raw water for example from 5 mg/l to 10 mg/l there is a decrease in the efficiency of biofilters, but the most relevant results are those at the end of the week, after normal operation of biofilters.

- The efficiency of the biological process is not significantly improved by the addition of phosphoric acid.
- Regarding the conformation of ammonium concentrations in biologically filtered water, at the maximum allowable concentration according to Law 458/2002, it can be said that in the case of biofilter with ceramic granules, at longer contact time between water and attached biomass, the ammonium concentration in filtered water was below 0.5 mg/l at concentration of 2 mg/l in raw water, and at a concentrations of 5 and 10 mg/l in raw water a maximum concentration of 0.59 mg/l in filtered water was obtained, close to the limit. For the other biofilters, good efficiencies were obtained at high contact time and low ammonium concentrations in raw water, but when the contact time was reduced, the efficiencies obtained were very low compared to the biofilter with ceramic granules.
- Biofilters can be used successfully in reducing ammonium concentrations in water, require low operating costs, and in the case of concentrations close to the limit, a secondary treatment with chlorination at breakpoint can be used, but the required doses of chlorine would be much lower than a direct treatment with chlorine (without biofilters).

References

[1] United States Environmental Protection Agency 2010 *Nutrient Control - Design Manual* (Office of Research and Development)
[2] United States Environmental Protection Agency 1993 *Manual - Nitrogen Control* (Office of Research and Development)
[3] Radu G 2018 *Raport de cercetare: Inventarul surselor de apa cu continut ridicat de amoniu din Romania* (Bucharest: Technical University of Civil Engineering of Bucharest)
[4] Qinli W, Yuanyuan Z, Wangxi L, Ruili L, Qihua H, Xiaohong F, Roberto D M, Cindy A, Nicolaus W and Jinxing L 2013 Single-particle analysis reveals shutoff control of the Arabidopsis ammonium transporter AMT1;3 by clustering and internalization *Proc. Natl. Acad. Sci. U.S.A.* **110**
[5] Degrémont 1991 *Water Treatment Handbook* vol 6 (Paris: Rueil-Malmaison)
[6] Hong Z, Lijie H, Hongwen M, Yan Z, Hongmei Z, Donghong L and Shuping L 2008 Adsorption characteristics of ammonium ion by zeolite 13X *J. Hazard. Mater.* **158** 577-584
[7] World Health Organization 1996 *Ammonia drinking-water. Background document for development of WHO Guidelines for drinking-water quality* (Geneva)
[8] Monitorul Oficial al Romaniei 2011 *Lege nr. 458 din 8 iulie 2002*
[9] European Parliament and of the Council 2020 *Directive EU 2184*
[10] Julio A C and Alvaro A 2006 Ecological and toxicological effects of inorganic nitrogen pollution in aquatic ecosystems: A global assessment *Environ. Int.* **32** 831-849
[11] Huang J, Kankanamge N R, Chow C, Welsh D T, Li T and Teasdale P R 2018 Removing ammonium from water and wastewater using cost-effective adsorbents *J. Environ. Sci. (China)* **63** 174-97
[12] Grady C P L Jr, Daigger G T, Love N G and Filipe C D M 2011 *Biological Wastewater Treatment* vol 3 (IWA Publishing and CRC Press)
[13] Chermisinoff N P 1996 *Biotechnology for Waste and Wastewater Treatment* (United States of America: Noyes Publications)
[14] Calin C 2011 *Teza de doctorat: Procese si Tehnologii pentru Controlul Continutului de Azot din Apa* (Bucharest: Technical University of Civil Engineering of Bucharest)
[15] Radu G and Racoviteanu G 2021 Removing ammonium from water intended for human consumption. A review of existing technologies *Earth Environ. Sci.* **664**
[16] Xu L, Campos L A C, Canales M and Ciric L 2020 Drinking water biofiltration: Behaviour of antibiotic resistance genes and the association with bacterial community *Water Res.* **182**

Hibrid system energetic performances evaluation composed by vapor compression heat pump used in building heating and dailly hot water

Evaluarea performantelor energetice a sistemului hibrid compus din pompa de caldura cu compresie de vapori utilizata in incalzirea cladirilor si apa zilnica

Florin Iordache[1], Mugurel Talpiga[2], Alexandru Draghici[3]

[1,2,3] Universitatea Tehnică de Construcţii Bucureşti
Bd. Lacul Tei nr. 122 - 124, cod 020396, Sector 2, Bucureşti, România
E-mail: *fliord@yahoo.com, talpiga.mugurel@gmail.com*

DOI: 10.37789/rjce.2022.13.2.5

Abstract

This paper addresses the topic of wide interest, regarding the positive impact to environment by using renewable energy resources, in terms of building heatinf thermal agent and daily hot water preparation. Thus, a hydraulic scheme is proposed which consists of an air-water heat pump and a gas boiler that takes over the additional load in the conditions of external temperatures for which the heat pump cannot satisfy the entire needs of the consumer. In the first part of the analysis, the calculation procedure is structured with the necessary equations for the energy evaluations specific to each type of system, thus being possible to calculate the thermal input brought by each equipment. The method also summarizes the procedure for establishing Meteo data for the heating season, respectively for the entire year in terms of daily hot water consumption. The data thus structured are used to construct BINs that contain a number of hours characterized by an average temperature over the entire subinterval. After establishing the working procedure and the BIN database, in the last part of the material two examples were proposed, for both situations in which an air-to-water heat pump of known dimensions is evaluated for establishing the energy coverage of a known consumer. The two examples address both heating and hot water consumption.

Key words: hibrid system, heat pump

1. Introduction

The implementation of the use of renewable sources is currently an intensely pursued objective in the context in which the use of hydrocarbon-based sources must be minimized as much as possible. This field includes the use of solar energy for the production of heat and electricity, the use of wind energy for the production of electricity, the use of biomass and biogas and the use of compression or absorption heat pumps to extract energy from the outside environment (air, apa, sol). The present paper follows a series of concerns in the field of the use of renewable resources, especially solar energy and the energy of the external environment. Some of the previous concerns in this field are mentioned in the bibliography of the paper.

The paper has a practical character, namely the presentation of the steps and steps to be performed to evaluate the energy contribution that a certain source system using the heat pump can offer to a specific consumer defined by its type and size. The previous papers mentioned in the bibliography substantiate the procedure presented in this paper.

The procedures presented take into account the fact that throughout the use of the compression heat pump, its coefficient of performance, COP, is variable depending on the temperatures of cold and hot environments and also the thermal power delivered to the pump condenser is variable depending on the electric power, absorbed at the heat pump compressor. One assumption used in the procedures is the constant value of the average temperature differences at the heat pump evaporator and condenser, Δt_{VP} and Δt_{CD}, respectively.

The procedures involve the construction of BIN type outdoor temperature ranges and the establishment within each such range of the COP of the heat pump and the electrical power used. At each BIN type interval, the thermal powers delivered by the heat pump and the classic source, the thermal power plant, are established in order to cover the necessary thermal power of the consumer. The energy performance of the heat pump is represented by 2 parameters, namely an average value of the COP of the heat pump and the value of the thermal energy delivered by the heat pump during the operation period.

2. The procedure for evaluating the performance of the heat pump for heating the spaces of a residential type consumer.

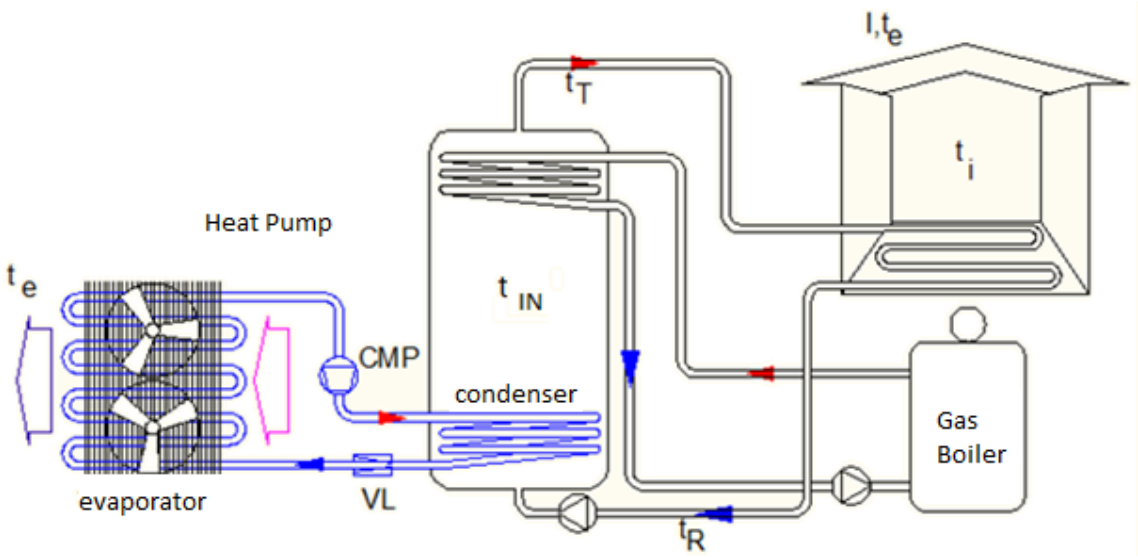

Fig.1

The description of the energy performance evaluation procedure will refer to the case of an air-water heat pump, in which the outside temperature intervenes both in the case of evaluating the thermal power delivered by the heat pump and in the case of evaluating the consumer's heat demand for space heating.

a. Input data :
   - Known data (proposed) : Δt_{VP} = 5 °C, Δt_{CD} = 5 °C, M = 0.958 si N = 1.5321;
   - Datashet heat-pump parameters :COP_0, θ_{VP0}, θ_{CD0}, P_{CD0}, η_{EL};
   - Building thermal characteristics : Φ_{INC0}, t_{T0}, t_{R0}, t_{i0}, t_{e0}:

b. Building thermal heat power evaluation and external themperature dependant thermal adjustment equations:

$$H_{INC} = \frac{\Phi_{INC\,0}}{\left(t_{i0} - t_{e0}\right)} \tag{1}$$

$$\Phi_{INC} = H_{INC} \cdot \left(t_{i0} - t_e\right) \tag{2}$$

$$t_T = \frac{t_{T0} - t_{e0}}{t_{i0} - t_{e0}} \cdot t_{i0} - \frac{t_{T0} - t_{i0}}{t_{i0} - t_{e0}} \cdot t_e \tag{3}$$

$$t_R = \frac{t_{R0} - t_{e0}}{t_{i0} - t_{e0}} \cdot t_{i0} - \frac{t_{R0} - t_{i0}}{t_{i0} - t_{e0}} \cdot t_e \tag{4}$$

c. Heat pump condenser and evaporator mathematical model equations:

$$\varepsilon_{VP}^{C} = \frac{\theta_{VP} - \Delta t_{VP} + 273.15}{\theta_{CD} - \theta_{VP} + \Delta t_{VP} + \Delta t_{CD}}$$
$$\varepsilon_{VP\_iz}^{*} = M \cdot \varepsilon_{VP}^{C} - N \tag{5}$$

$$\eta_{iz} = \frac{COP_0 - \eta_{EL}}{\varepsilon_{VP\_iz\_0}^{*} \cdot \eta_{EL}} \tag{6}$$

$$EER = \varepsilon_{VP\_iz}^{*} \cdot \eta_{iz} \cdot \eta_{EL}$$
$$COP = \left(1 + \varepsilon_{VP\_iz}^{*} \cdot \eta_{iz}\right) \cdot \eta_{EL} \tag{7}$$

$$P_{EL} = \frac{P_{CD}}{COP} \tag{8}$$

$$P_{VP} = P_{EL} \cdot EER$$
$$P_{CD} = P_{EL} \cdot COP \tag{9}$$

d. Based on known catalog conditions of the heat pump (COP_0, θVP_0, θ_{CD0}, P_{CD0}, η_{EL}) the refrigeration efficiency Carnot de calcul, $\varepsilon CVP0$ is established, using the relation (51) in these conditions and further computational isentropic refrigeration, $\varepsilon^{*}_{VP\_iz\_0}$, using the relation ($5_2$). Also, the isentropic efficiency of the compressor, η_{iz}, is further determined using the relation (6) and the catalog electric power of the heat pump using the relation (8) in catalog conditions.

e. Determining the outside temperature for which the heat pump manages to fully cover the heat required for heating the building spaces. This temperature is distinguished by the fact that it leads to equal values for the thermal power delivered by the heat pump condenser with the power needed to heat the building spaces: $P_{CD} = \Phi_{INC}$, ensuring the thermal balance of the heated spaces on the normal indoor temperature, t_{i0}. In order to determine the thermal power delivered by the condenser, the relation (9_2) will be used, where the COP of operation of the heat pump is established using the relations (5) and (7) where in the relation (5) it will be: θ_{VP} = tem, and $\theta_{CD} = t_{m0}$, where $t_{m0} = (t_{T0} + t_{R0}) / 2$. The relationship (2) will be used to determine the required heat flow of the consumer. We propose a graphical method for determining the external

equilibrium temperature, t_{eE}, by the intersection of the P_{CD} curves with Φ_{INC}, established graphically by points.

f. The following is the setting of the BIN outdoor temperature ranges. The outside equilibrium temperature, teE, divides the division of BIN intervals into 2 zones. Zone 1 of BIN intervals characterized by $t_e < t_{eE}$ outdoor temperatures and zone 2 of BIN intervals characterized by $t_e > t_{eE}$ outdoor temperatures. In zone 1 of BIN intervals the heat pump will absorb from the network an electric power equal to the catalog electric power of the heat pump but will provide the condenser with a thermal power lower than the power required by the consumer, the difference being covered by the boiler. In zone 2 BIN intervals the heat pump will absorb from the network a lower electric power than the catalog electric power by the intervention of the frequency converter and will deliver to the condenser a thermal power equal to the power required by the consumer. It is established for each BIN interval from zone 1 and from zone 2 the average external temperature of the respective BIN interval, tem. In the case of this paper, the determination of BIN intervals was done using a Meteo database. For a representative calendar year, the database contains 8760 temperature values corresponding to each hour and characterized by average hourly temperatures. The heating season corresponds to all the subperiods in which the average temperature for 3 days has a value of less than 12 ºC. Thus, a smaller number of hourly data is obtained, corresponding only to the heating period. Furthermore, the totality of the hours retained for the heating period, lead to the construction of the BIN intervals necessary to evaluate the operation of the heat pump. The construction of BIN intervals can be done by two methods.

Method 1 is represented by a number of predefined intervals. Each subinterval having the same length, established between the maximum, t_{e_max} and minimum temperatures, t_{e_min}, of the heating period, for a given number of necessary subintervals, according to the equation:

$$\Delta t_e = \frac{t_{e\_max} - t_{e\_min}}{n_i} \tag{10}$$

In which Δt_e represents the temperature step of each subinterval.

Method 2 is represented by a number of equal sub-intervals for which the temperature step is this time predetermined and the number of sub-intervals being calculated according to the equation:

$$n_i = \frac{t_{e\_max} - t_{e\_min}}{\Delta t_e} \tag{11}$$

Both methods generate BIN intervals, characterized by an average temperature between the ends of the subintervals calculated with the temperature step set according to Method 1 or predetermined by Method 2. Obviously each BIN will contain all the hours in the database, related to the heating period, which have as temperature hourly average, a value within its characteristic temperature subinterval.

g. To determine the effective operation of the heat pump within the BIN intervals in zone 1, proceed to each of the BIN intervals in this zone as follows:
- It is proposed a degree of energy coverage for the heat pump, GAPC:
- The temperature of the warm environment is determined according to the relation

$$\theta_{CD} = 0.5 \cdot GA_{PC} \cdot t_T + \left(1 - 0.5 \cdot GA_{PC}\right) \cdot t_R \tag{12}$$

- The operating COP of the heat pump is established according to relations (5) and (7);
- It is established the thermal power yielded by the heat pump to the P_{CD} condenser and the heat demand of the house, Φ_{INC}, at the external temperature, tem, according to relations (9_2) and (2);
- Calculate the energy coverage of the heat pump, GAPC:

$$GA_{PC} = \frac{P_{CD}}{\Phi_{INC}} \tag{13}$$

- Returning with the value resulting from the application of the relation (13) for the GA_{PC} in the relation (12) is obtained in this way a rapidly recurring convergent series of GA_{PC} values.
- - The final value obtained for the energy coverage degree, GA_{PC}, has previously calculated the value of EER and COP, and the powers of P_{CD}, P_{VP}, P_{EL} and Φ_{INC},
- - The energies corresponding to the respective BIN intervals are further established:

$$\begin{aligned} E_{CD} &= \Delta\tau_{BIN} \cdot P_{CD} / 1000 \\ E_{VP} &= \Delta\tau_{BIN} \cdot P_{VP} / 1000 \\ E_{EL} &= \Delta\tau_{BIN} \cdot P_{EL} / 1000 \\ E_{INC} &= \Delta\tau_{BIN} \cdot \Phi_{INC} / 1000 \end{aligned} \tag{14}$$

- We can also define a green energy coverage :

$$GA_{VP} = \frac{P_{VP}}{\Phi_{INC}} \tag{15}$$

h. To determine the effective operation of the heat pump within the BIN intervals in zone 2, proceed to each of the BIN intervals in this zone as follows:
- The thermal power delivered to the condenser of the heat pump, P_{CD}, is established as equal to the required thermal flow of the consumer, Φ_{INC},
- The operating COP of the heat pump is established according to relations (5) and (7);
- The electric power absorbed from the network is established according to the relation (8);
- The degree of energy coverage, GA_{PC}, is 1 and based on the relation (91) the thermal power absorbed at the vaporizer, P_{VP} is established;
- The energies corresponding to the respective BIN intervals are further established using the relations (14) and the degree of green energy coverage according to the relation (15);
- Finally, it is established by summing up the situation at the level of the entire cold season of the year regarding the energies: total thermal energy necessary for the consumer, $E_{INC\text{-}year}$, total thermal energy delivered by the heat pump, $E_{CD\text{-}year}$, total electricity absorbed by mains heat pump, $E_{EL\text{-}year}$, the total thermal energy absorbed by the heat pump evaporator, $E_{VP\text{-}year}$ and the total thermal energy supplied by the boiler, $E_{CT\text{-}an}$. It also shows the degrees of annual energy coverage, $GA_{PC\text{-}year}$, $GA_{VP\text{-}year}$, $GA_{CT\text{-}year}$.

3. Procedure for evaluating the performance of the heat pump for the preparation of hot water for the consumption of a residential consumer.

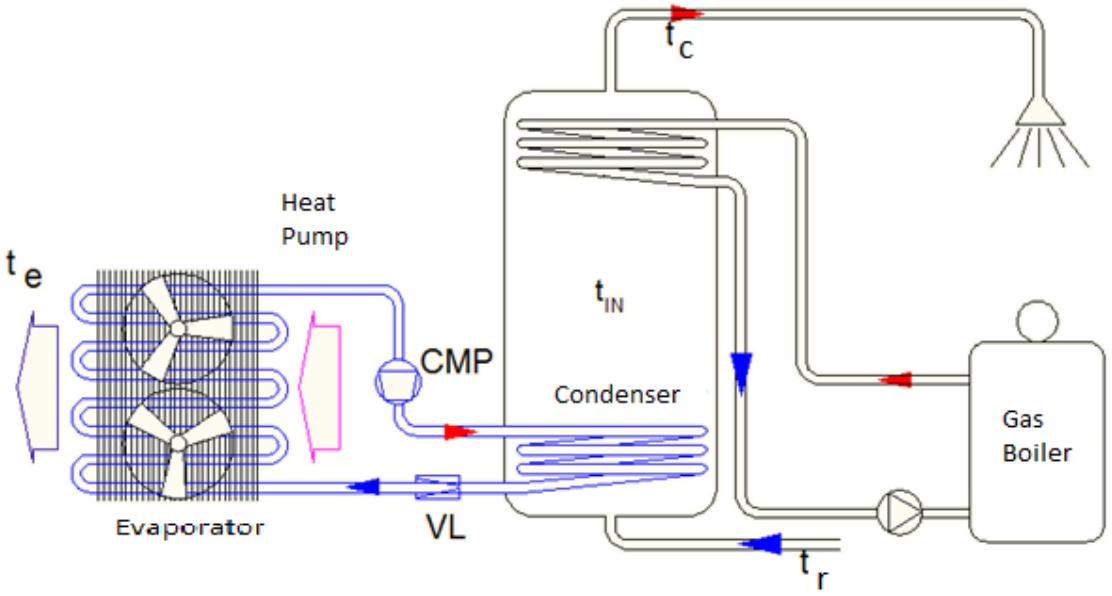

Fig. 2

The description of the energy performance evaluation procedure will refer to the case of an air-to-water heat pump, in which the outside temperature intervenes in the case of the evaluation of the thermal power delivered by the heat pump.

a. Input data:
   - Known parameters : Δt_{VP} = 5 °C, Δt_{CD} = 5 °C, M = 0.958 si N = 1.5321;
   - Heat pump datasheet known parameters :COP_0, θ_{VP0}, θ_{CD0}, P_{CD0}, η_{EL};
   - Building thermal characteristics : G_{ACC}, t_{ac}, t_{ar} :

b. Building thermal heat power evaluation and external themperature dependant thermal adjustment equations:

$$H_{ACC} = 1.163 \cdot G_{ACC} \tag{1}$$

$$\Phi_{ACC} = H_{ACC} \cdot \left(t_c - t_r\right) \tag{2}$$

c. Heat pump evaporation and condensing thermal power evaluation equations :

$$\varepsilon_{VP}^{C} = \frac{\theta_{VP} - \Delta t_{VP} + 273.15}{\theta_{CD} - \theta_{VP} + \Delta t_{VP} + \Delta t_{CD}}$$
$$\varepsilon_{VP\_iz}^{*} = M \cdot \varepsilon_{VP}^{C} - N \tag{3}$$

$$\eta_{iz} = \frac{COP_0 - \eta_{EL}}{\varepsilon_{VP\_iz\_0}^{*} \cdot \eta_{EL}} \tag{4}$$

$$EER = \varepsilon_{VP\_iz}^{*} \cdot \eta_{iz} \cdot \eta_{EL}$$
$$COP = \left(1 + \varepsilon_{VP\_iz}^{*} \cdot \eta_{iz}\right) \cdot \eta_{EL} \tag{5}$$

$$P_{EL} = \frac{P_{CD}}{COP} \tag{6}$$

$$P_{VP} = P_{EL} \cdot EER$$
$$P_{CD} = P_{EL} \cdot COP \tag{7}$$

d. Based on the knowledge of the catalog conditions of the heat pump (COP0, θ_{VP0}, θ_{CD0}, P_{CD0}, η_{EL}) the refrigeration efficiency Carnot de calcul, ε^{C}_{VP0} is established, using the relation (3_1) in these conditions and further the isentropic refrigeration efficiency of calculation, $\varepsilon^{*}_{VP\_iz\_0}$, using relation ($3_2$). Also, the isentropic efficiency of the compressor, η_{iz}, is further determined using the

relation (4) and the catalog electric power of the heat pump using the relation (6) in catalog conditions.

e. Determining the outdoor temperature for which the heat pump manages to fully cover the heat required for the preparation of hot water for the building. This temperature is distinguished by the fact that it leads to equal values for the thermal power delivered by the heat pump condenser with the power required to heat the building spaces: $P_{CD} = \Phi_{ACC}$. To determine the thermal power delivered by the condenser we will use the relation (7_2) where the COP of operation of the heat pump is established using the relations (3) and (5) where in the relation (3) we will have: $\theta_{VP} = t_e$, and $\theta_{CD} = (t_c + t_r)/2$.

The relationship (2) will be used to determine the required heat flow of the consumer. We propose a graphical method for determining the equilibrium external temperature, t_{eE}, by the intersection of the P_{CD} curves with Φ_{ACC}, established graphically by points.

f. Next is the evaluation of the BIN intervals of the external temperature. The equilibrium external temperature, teE, divides the division of BIN intervals into 2 zones. Zone 1 of BIN intervals characterized by $t_e<t_{eE}$ outdoor temperatures and zone 2 of BIN intervals characterized by $t_e>t_{eE}$ outdoor temperatures. In zone 1 of BIN intervals the heat pump will absorb from the network an electric power equal to the catalog electric power of the heat pump but will provide the condenser with a thermal power lower than the power required by the consumer, the difference being covered by the boiler. In zone 2 BIN intervals the heat pump will absorb from the network a lower electric power than the catalog electric power by the intervention of the frequency converter and will deliver to the condenser a thermal power equal to the power required by the consumer. It is established for each BIN interval from zone 1 and from zone 2 the average external temperature of the respective BIN interval, tem. And in the case of preparing hot water for consumption, the procedure for establishing the BIN intervals is based on the hourly data generated with the help of the Meteo database. Also, the two methods described above for the heating system can be applied exactly for hot water. The specification that needs to be made represents the full use of the hours in the generated database, the period of use of hot drinking water being all year round.

g. To determine the effective working mode of the heat pump within the BIN intervals in zone 1, proceed to each of the BIN intervals in this zone as follows:
   - We propose a heat pump coverage energy ratio, GA_{PC}:
   - We evaluate condensing energy by :

$$\theta_{CD} = 0.5 \cdot GA_{PC} \cdot t_c + \left(1 - 0.5 \cdot GA_{PC}\right) \cdot t_r \quad (8)$$

- We establish COP with equations (3) si (5);
- We establish condensing thermal power, P_{CD}, and building power demand according external temperature, t_e, with equations (7_2) si (2);
- Coverage energy ratio is again evaluated with:

$$GA_{PC} = \frac{P_{CD}}{\Phi_{ACC}} \tag{9}$$

- Re turning with the value resulting from the application of relation (9) for GA_{PC} in relation (8) is obtained in this way a rapidly recurring convergent series of GA_{PC} values.
- The final value obtained for the energy coverage degree, GA_{PC}, has previously calculated the value of EER and COP, and the powers of P_{CD}, P_{VP}, P_{EL} and Φ_{ACC},
- The energies corresponding to the respective BIN intervals are further established:

$$\begin{aligned} E_{CD} &= \Delta\tau_{BIN} \cdot P_{CD} / 1000 \\ E_{VP} &= \Delta\tau_{BIN} \cdot P_{VP} / 1000 \\ E_{EL} &= \Delta\tau_{BIN} \cdot P_{EL} / 1000 \\ E_{ACC} &= \Delta\tau_{BIN} \cdot \Phi_{ACC} / 1000 \end{aligned} \tag{10}$$

- Can be defined an coverage green energy ratio:

$$GA_{VP} = \frac{P_{VP}}{\Phi_{ACC}} \tag{11}$$

h. To determine the effective operation of the heat pump within the BIN intervals in zone 2, proceed to each of the BIN intervals in this zone as follows:

- The thermal power delivered to the condenser of the heat pump, P_{CD}, is established as being equal to the required thermal flow of the consumer, Φ_{ACC},

- The operating COP of the heat pump is established according to relations (3) and (5);

- The electric power absorbed from the network is established according to the relation (6);

- The degree of energy coverage, GA_{PC}, is 1 and based on the relation (7_1) the thermal power absorbed at the vaporizer, P_{VP} is established;

- The energies corresponding to the respective BIN intervals are further established using the relations (10) and the degree of green energy coverage according to the relation (11);

- Finally, it is established by summation, the situation at the level of the entire cold season of the year in terms of energy: total thermal energy required by the consumer, $E_{INC\text{-}year}$, total thermal energy delivered by heat pump, $E_{CD\text{-}year}$, total electricity absorbed by mains heat pump, $E_{EL\text{-}an}$, the total thermal energy absorbed by the heat pump evaporator, $E_{VP\text{-}an}$ and the total thermal energy provided by the thermal power plant, $E_{CT\text{-}year}$. The results of the annual energy coverage, $GA_{PC\text{-}year}$, $GA_{VP\text{-}year}$, $GA_{CT\text{-}year}$ also result

4. Examples

In order to have a more correct understanding of the calculation procedures, the following is an example of a calculation for the procedure of space heating and hot water preparation. It is considered a residential building located in the town of Toplita.

On the heating side of the spaces, this building is characterized by a computational heat demand Φ_{INC0} = 200000 W. The central heating installation was dimensioned at the nominal parameters of the thermal agent t_{T0} = 90ºC, t_{R0} = 70ºC. The normalized indoor temperature is t_{i0} = 20ºC, and the calculated outdoor temperature is t_{e0} = -21ºC. The heat pump is characterized by COP_0 = 2.5, θ_{VP0} = 2 ºC, θ_{CD0} = 60 ºC, P_{CD0} = 150000 W, η_{EL} = 0.95.

For the effective application of the procedure for evaluating the energy performance of the use of the heat pump, a calculation program was built in SCILAB. According to the presented data, the value of t_{eE} = - 8.78 ºC resulted in the case of heating the building spaces, for the external equilibrium temperature.

Next can be graphically followed the simulation results.

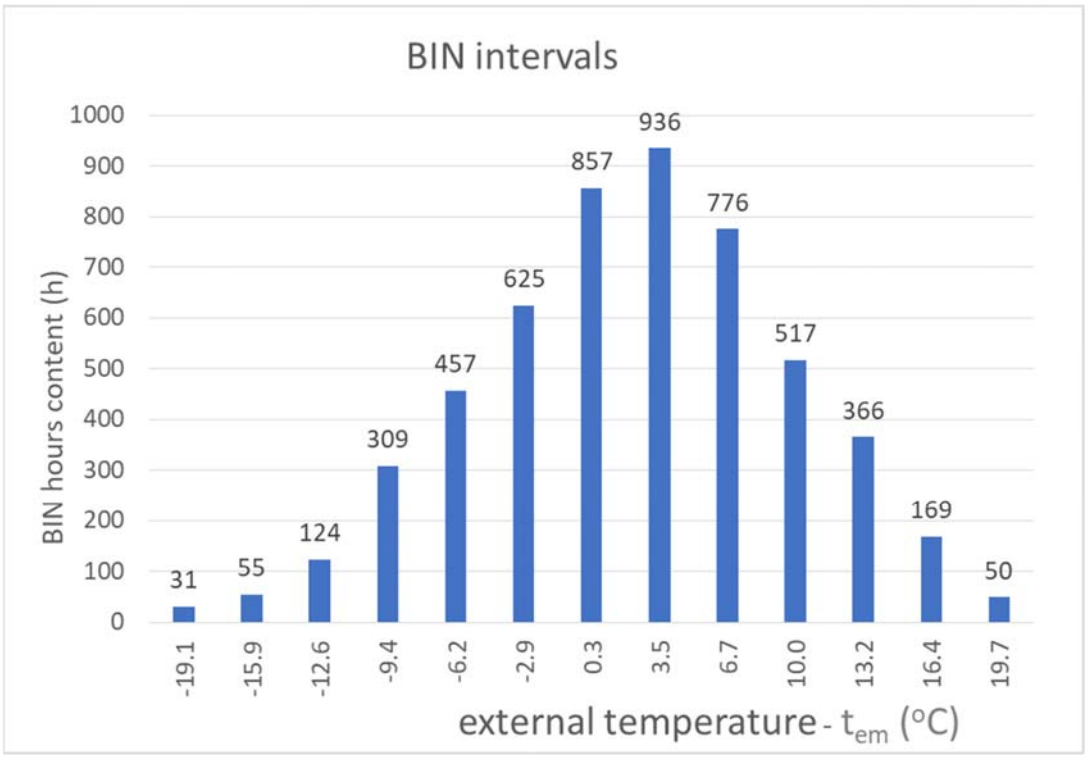
BIN intervals
BIN hours content (h)
1000
900
800
700
600
500
400
300
200
100
0
31
55
124
309
457
625
857
936
776
517
366
169
50
-19.1
-15.9
-12.6
-9.4
-6.2
-2.9
0.3
3.5
6.7
10.0
13.2
16.4
19.7
external temperature - t_{em} (°C)

Fig.3

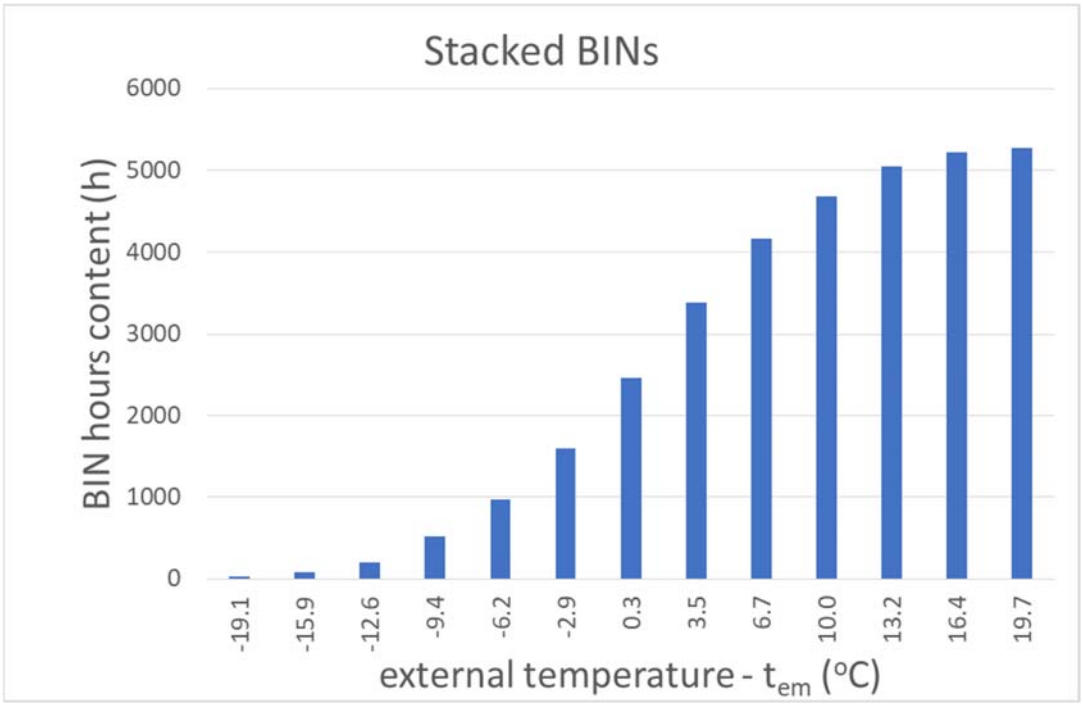
Stacked BINs
BIN hours content (h)
6000
5000
4000
3000
2000
1000
0
-19.1
-15.9
-12.6
-9.4
-6.2
-2.9
0.3
3.5
6.7
10.0
13.2
16.4
19.7
external temperature - t_{em} (°C)

Fig.4

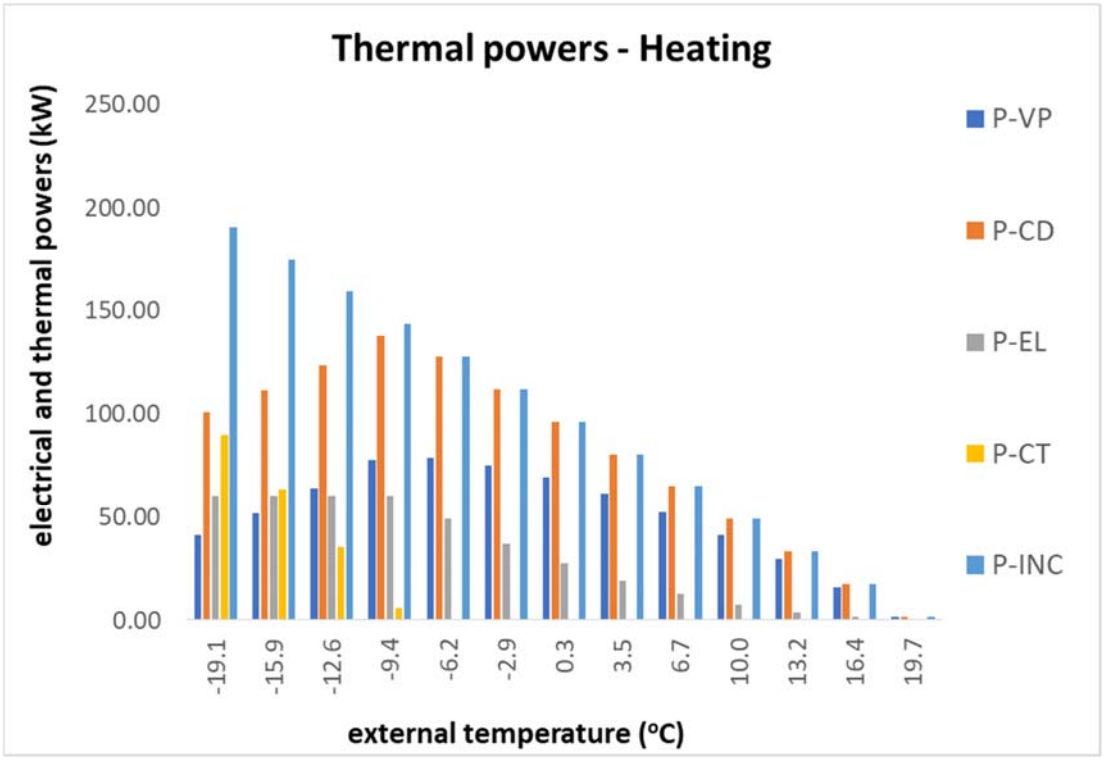
Thermal powers - Heating
electrical and thermal powers (kW)
250.00
200.00
150.00
100.00
50.00
0.00
-19.1
-15.9
-12.6
-9.4
-6.2
-2.9
0.3
3.5
6.7
10.0
13.2
16.4
19.7
external temperature (°C)
P-VP
P-CD
P-EL
P-CT
P-INC

Fig.5

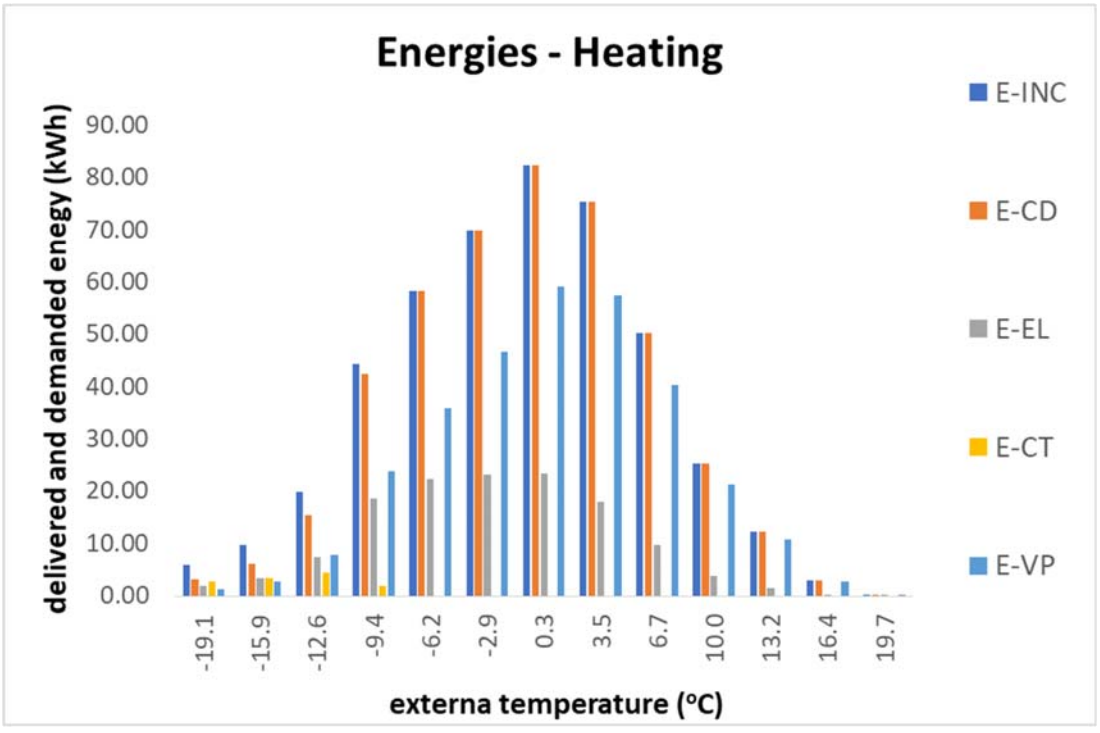
Energies - Heating
delivered and demanded enegy (kWh)
90.00
80.00
70.00
60.00
50.00
40.00
30.00
20.00
10.00
0.00
-19.1
-15.9
-12.6
-9.4
-6.2
-2.9
0.3
3.5
6.7
10.0
13.2
16.4
19.7
externa temperature (°C)
E-INC
E-CD
E-EL
E-CT
E-VP

Fig.6

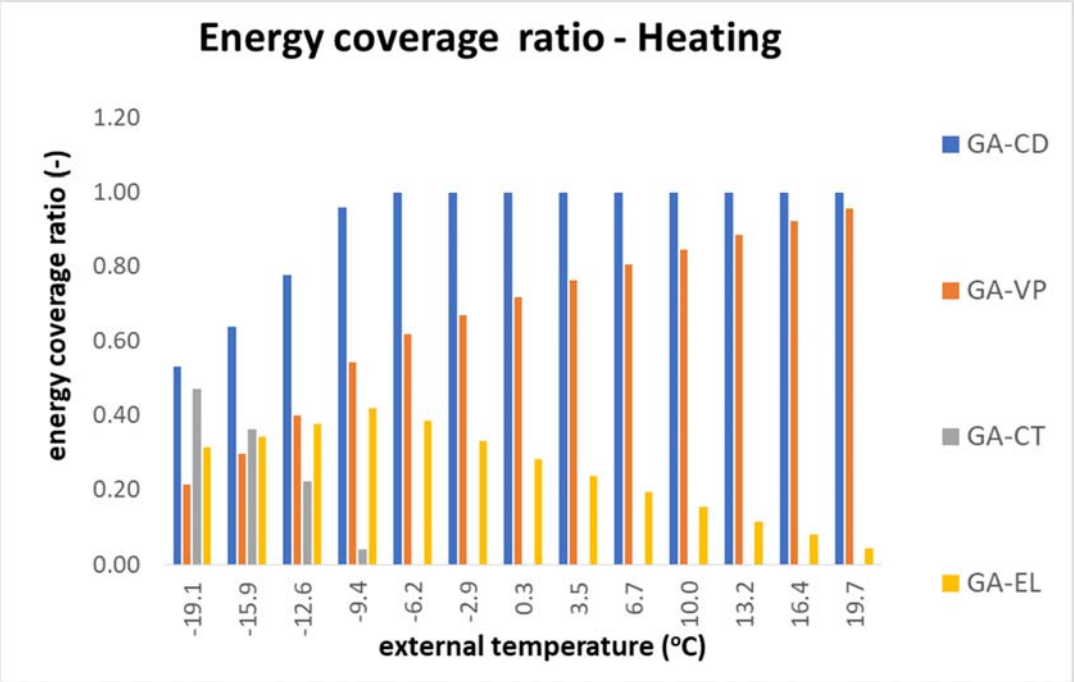
Energy coverage ratio - Heating
energy coverage ratio (-)
1.20
1.00
0.80
0.60
0.40
0.20
0.00
-19.1
-15.9
-12.6
-9.4
-6.2
-2.9
0.3
3.5
6.7
10.0
13.2
16.4
19.7
external temperature (°C)
GA-CD
GA-VP
GA-CT
GA-EL

Fig.7

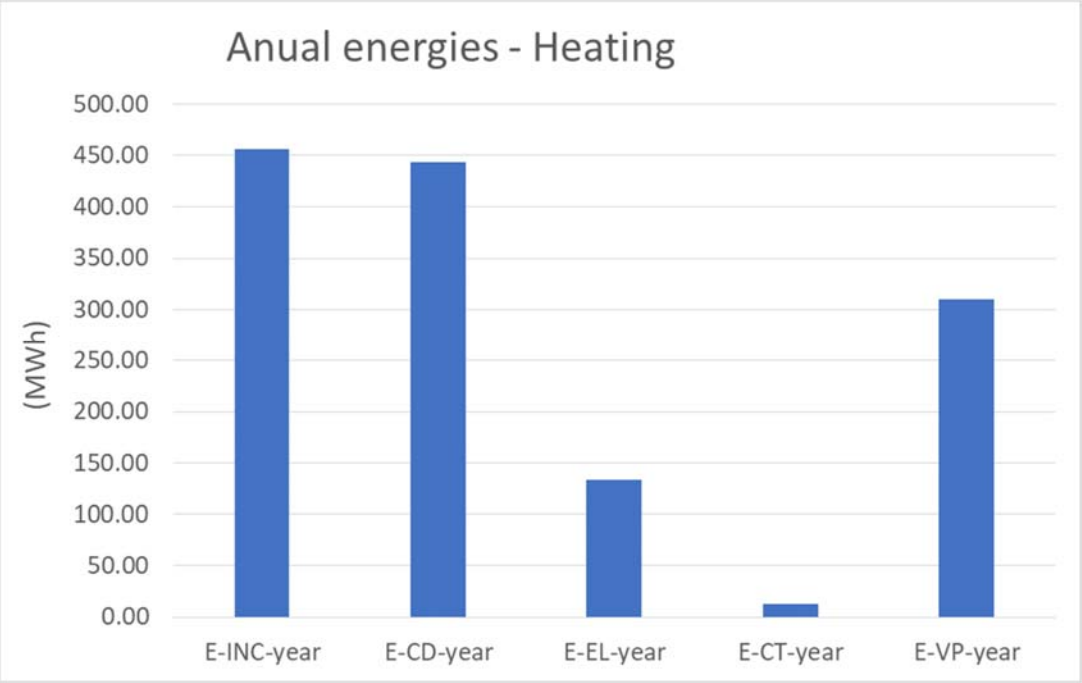
Anual energies - Heating
(MWh)
500.00
450.00
400.00
350.00
300.00
250.00
200.00
150.00
100.00
50.00
0.00
E-INC-year
E-CD-year
E-EL-year
E-CT-year
E-VP-year

Fig.8

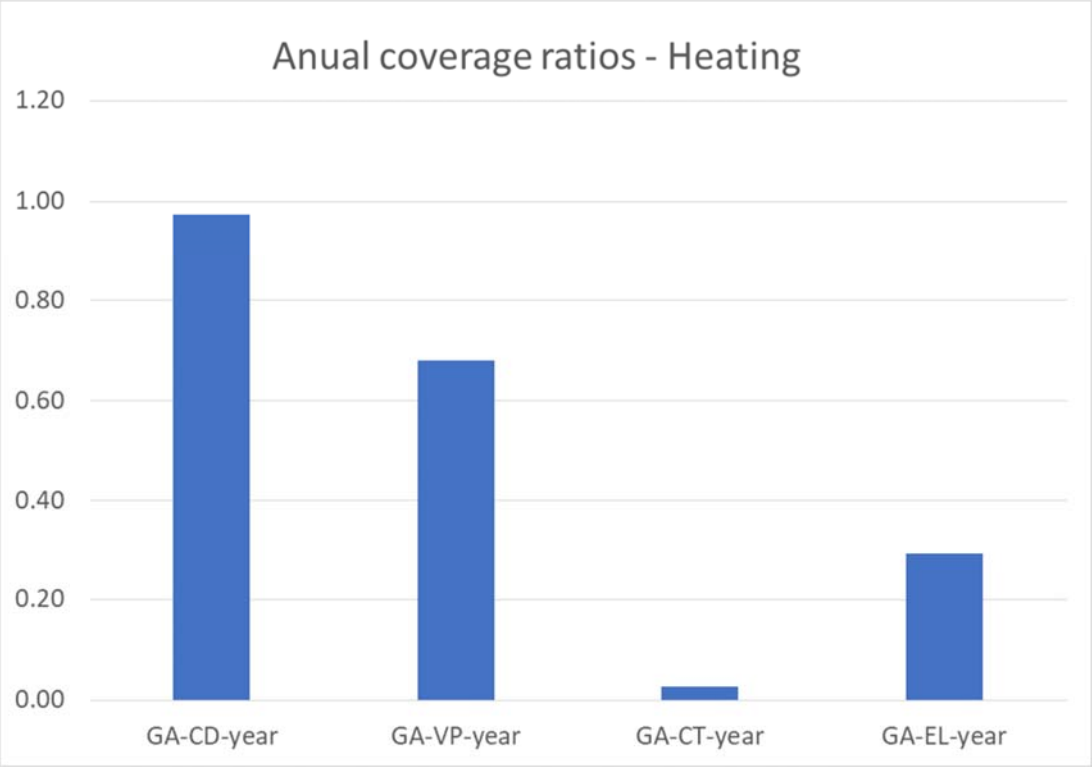

Fig.9

On the hot water supply side, this building is characterized by a consumption of hot water consumption of 110 /persons.day, in the building living 120 people. The hot water preparation installation was dimensioned at the nominal parameters of the thermal agent t_c = 55 °C, t_r = 10 °C. The heat pump is characterized by COP_0, = 2.5, θ_{VP0} = -5 °C, θ_{CD0} = 60 °C, P_{CD0} = 12000 W, η_{EL} = 0.95, Toplita locality. BIN data for the whole year are used to calculate the heat demand, the total number of hours being 8760.

For the effective application of the procedure for evaluating the energy performance of the use of the heat pump, a calculation program in SCILAB was built, as in the case of space heating. According to the presented data, the value of teE = +5.68 °C resulted in the case of preparing the hot water for consumption related to the building.

Simulation results graphics.

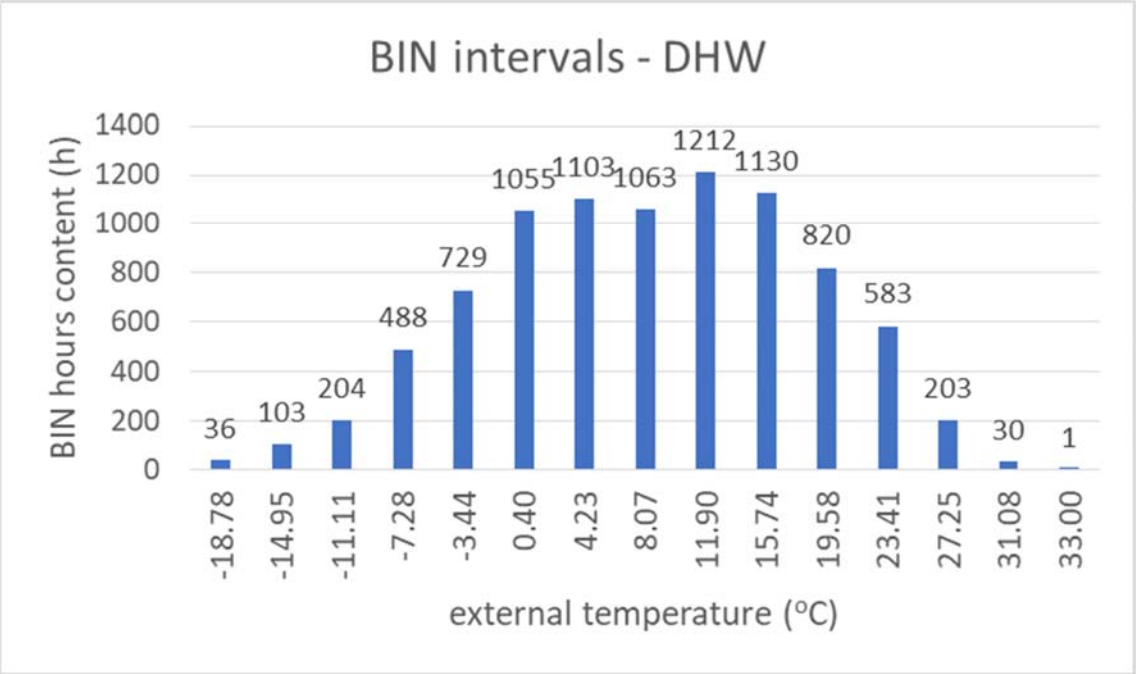
BIN intervals - DHW
BIN hours content (h)
1400
1200
1000
800
600
400
200
0
36
103
204
488
729
1055
1103
1063
1212
1130
820
583
203
30
1
-18.78
-14.95
-11.11
-7.28
-3.44
0.40
4.23
8.07
11.90
15.74
19.58
23.41
27.25
31.08
33.00
external temperature (°C)

Fig. 10

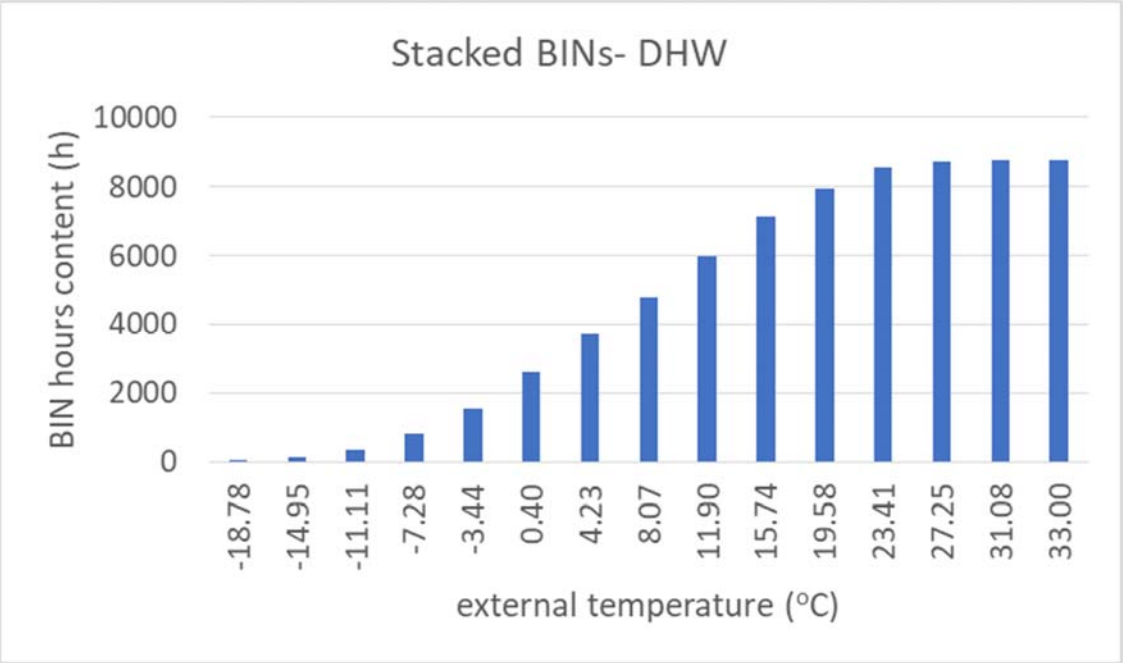
Stacked BINs- DHW
BIN hours content (h)
10000
8000
6000
4000
2000
0
-18.78
-14.95
-11.11
-7.28
-3.44
0.40
4.23
8.07
11.90
15.74
19.58
23.41
27.25
31.08
33.00
external temperature (°C)

Fig. 11

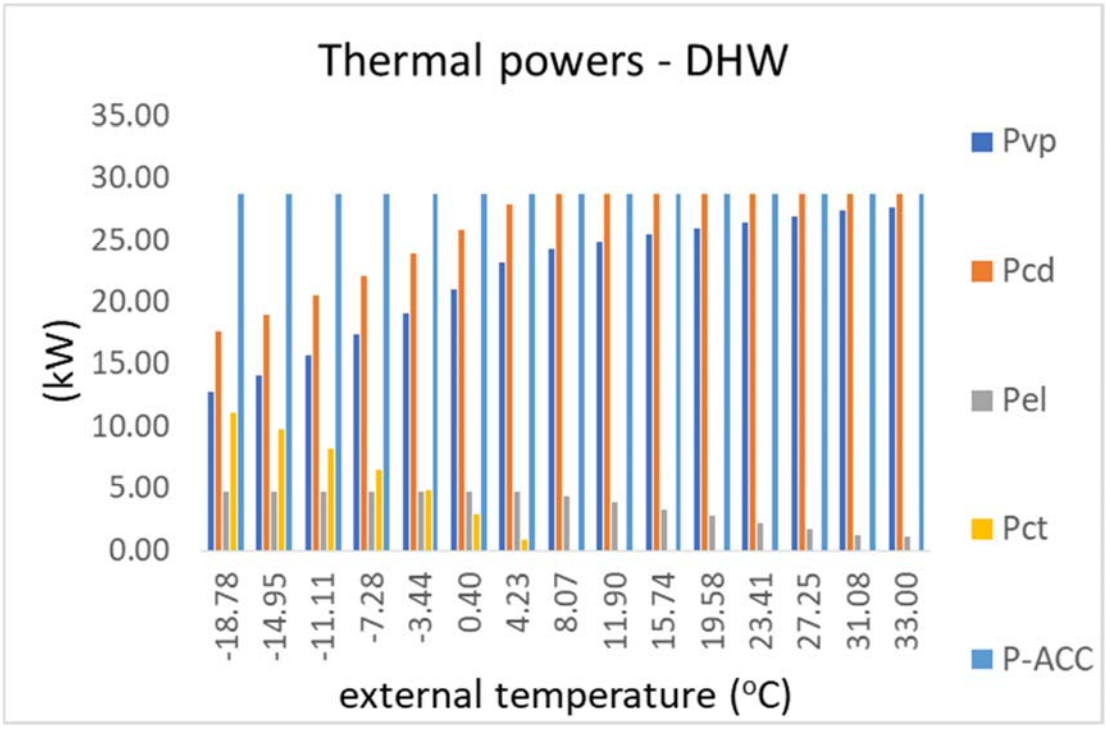
Thermal powers - DHW
35.00
30.00
25.00
20.00
15.00
10.00
5.00
0.00
(kW)
-18.78
-14.95
-11.11
-7.28
-3.44
0.40
4.23
8.07
11.90
15.74
19.58
23.41
27.25
31.08
33.00
external temperature (ºC)
Pvp
Pcd
Pel
Pct
P-ACC

Fig. 12

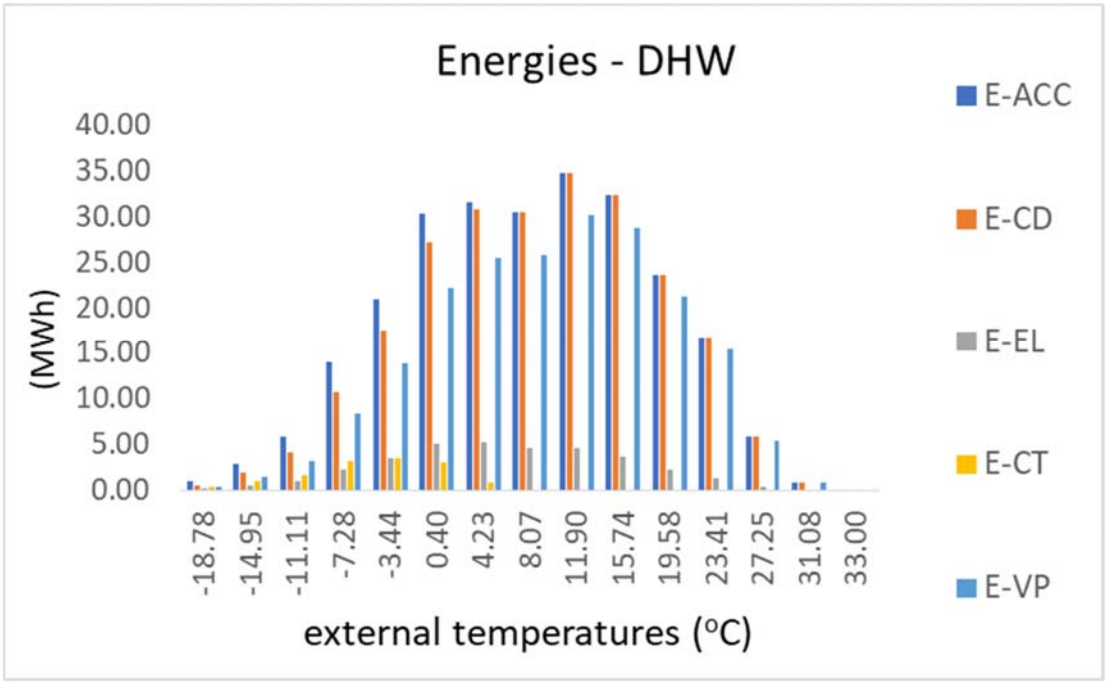
Energies - DHW
40.00
35.00
30.00
25.00
20.00
15.00
10.00
5.00
0.00
(MWh)
-18.78
-14.95
-11.11
-7.28
-3.44
0.40
4.23
8.07
11.90
15.74
19.58
23.41
27.25
31.08
33.00
external temperatures (ºC)
E-ACC
E-CD
E-EL
E-CT
E-VP

Fig. 13

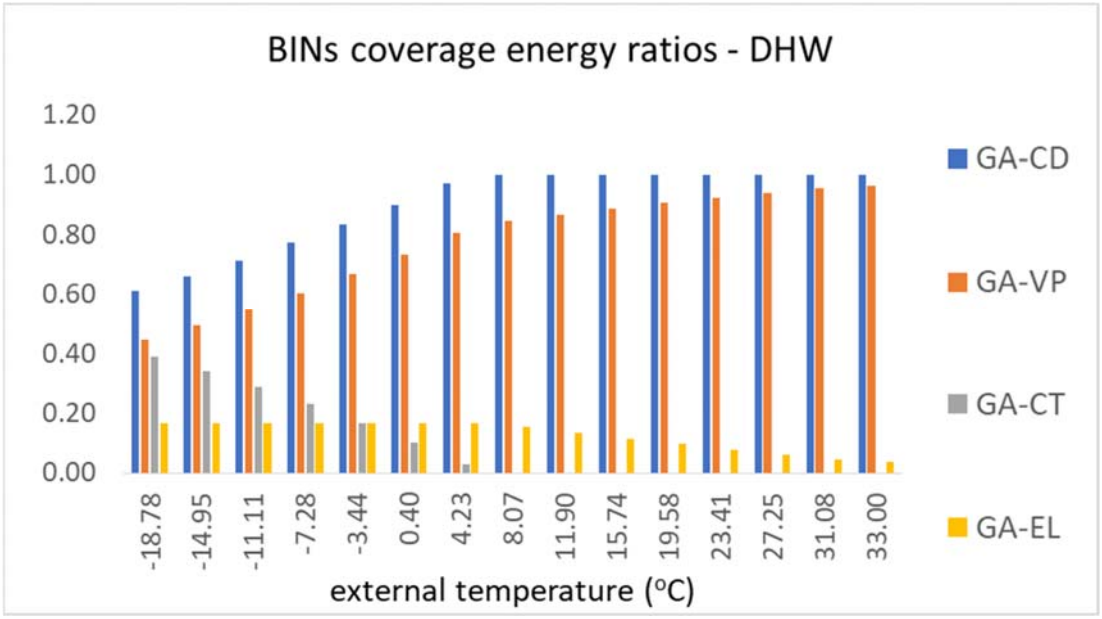
BINs coverage energy ratios - DHW
1.20
1.00
0.80
0.60
0.40
0.20
0.00
-18.78
-14.95
-11.11
-7.28
-3.44
0.40
4.23
8.07
11.90
15.74
19.58
23.41
27.25
31.08
33.00
external temperature (°C)
GA-CD
GA-VP
GA-CT
GA-EL

Fig. 14

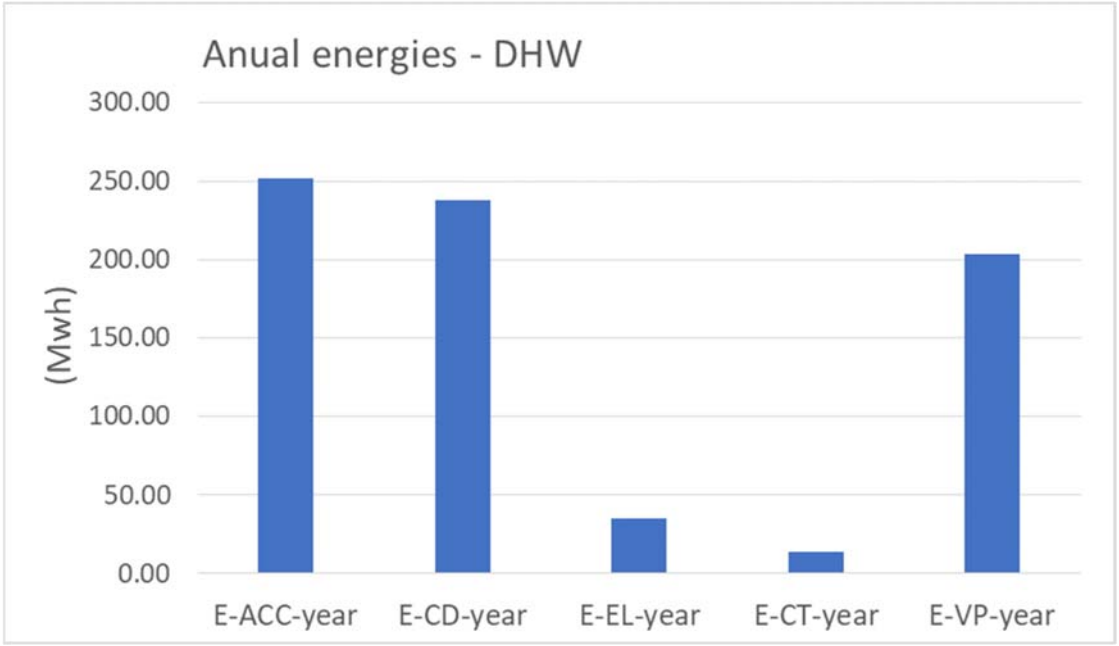
Anual energies - DHW
300.00
250.00
200.00
150.00
100.00
50.00
0.00
(Mwh)
E-ACC-year
E-CD-year
E-EL-year
E-CT-year
E-VP-year

Fig. 15

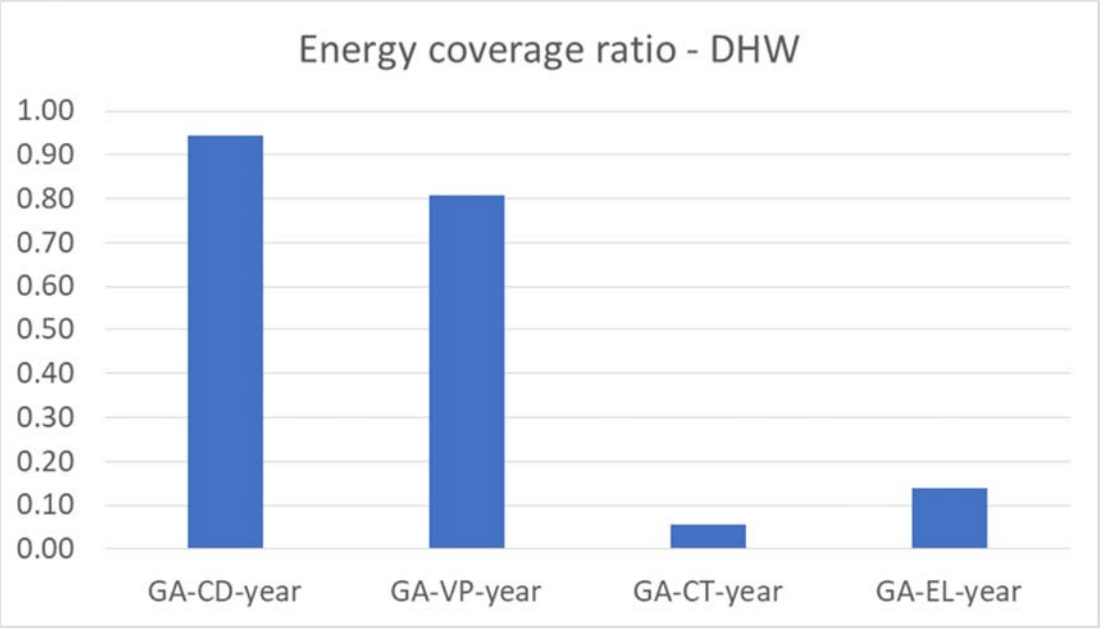

Fig. 16

5. Conclusions

For the effective application of the procedure for evaluating the energy performance of the use of the heat pump, a calculation program in SCILAB was built, as in the case of space heating. According to the data presented, the value of t_{eE} = +5.68 ºC, as presented from the beginning, for the external equilibrium temperature for the building, resulted in the preparation of hot drinking water related to the building. a heat pump in a hybrid system next to a thermal power plant, for servicing a central heating installation of a building's spaces and separately for servicing a domestic hot water preparation installation.

There are 4 basic steps:

- determination of the equilibrium outside temperature (which involves an iterative calculation),
- construction of BIN outdoor temperature ranges;
- establishing the energy inputs brought by the heat pump within the BIN intervals characterized by outside temperatures lower than the outside equilibrium temperature (involves an iterative calculation);
- establishing the energy inputs brought by the heat pump within the BIN intervals characterized by outdoor temperatures higher than the outside equilibrium temperature;
- the annual balance of the energy contributions brought by the heat pump;

Taking into account the series of calculations to be performed and taking into account the iterative determinations to be made in the mentioned steps, the use of an automatic calculation program is absolutely necessary. We mention the fact that it is possible to use the excel work environment even if certain stages are solved a little slower. In the final stage, the energies provided by the heat pump, by the environment from which the heat is extracted, by the thermal power plant using fossil fuel are cumulated throughout. The total electricity consumption is also evaluated and it is related to the necessary energy consumption of the consumer.

Nomenclature:

t_{i0} – interior standard temperature, ^oC;
t_{e0} – exterior calculation standard temperature, ^oC;
t_{T0} – maximum heating agent calculation temperature, ^oC;
t_{R0} – maximum return heating agent temperature, ^oC;
t_{m0} – average thermal agent calculation temperature, ^oC;
t_T – heating agent out temperature, ^oC;
t_R – return heating agent temperature, ^oC;
t_e – external temperature, ^oC;
t_{em} – BIN average temperature, ^oC;
t_{eE} – balance external temperature, ^oC;
t_c – daily hot water set temperature, ^oC;
t_r – water source cold temperature, ^oC;
Δt_{VP} – evaporator logarithmic average temperature difference, ^oC;
Δt_{CD} – condensing logarithmic average temperature, ^oC;
θ_{VP0} – datasheet known evaporation environment temperature, ^oC;
θ_{CD0} – datasheet known condensing environment temperature, ^oC;
θ_{VP} – evaporation environment temperature, ^oC;
θ_{CD} – condensing environment temperature, ^oC;
G_{ACC} – daily hot water flow rate, l/h;
P_{VP} – evaporation thermal power, W;
P_{CD} – condensing thermal power, W;
Φ_{INC} – building heating demand, W;
Φ_{INC0} – maximum building heating demand, W;
Φ_{ACC} – daily hot water heating demand, W;
P_{EL} – compressor electrical power, W;
E_{VP} – evaporation thermal energy, kWh;
E_{CD} – condensing thermal energy, kWh;
E_{EL} – electrical energy, kWh;
E_{INC} – heating energy, kWh;

E_{ACC} – daily hot water heating energy, kWh;
H_{INC} – building heat transfer coefficient, W/K;
H_{ACC} – consumer daily hot water heat transfer coefficient, W/K;
$\Delta\tau_{BIN}$ – BIN interval number of hours, h;
ε^{C}_{VP} – Carnot efficiency, -;
$\varepsilon^{*}_{VP\_iz}$ – calculated isentropic efficiency, -;
$\varepsilon^{*}_{VP\_iz\_0}$ – datasheet isentropic efficiency of heatpump , -;
EER – energy efficiency ratio, -;
COP – coefficient of performance, -;
COP_0 – heat pump datasheet coefficient of performance, -;
η_{iz} – isentropic compressor efficiency, -;
η_{EL} – compressor electrical drive efficiency, -;
GA_{PC} – heat pump coverage energy ratio, -;
GA_{VP} – heat pump coverage green energy ratio, -;
M, N – constants, -;

References:

1. Florin Iordache, Mugurel Talpiga - Aspecte privind optimizarea constructiv-functionala a unui sistem de pompa de caldura cu compresie (cu sursa de rezerva) pentru incalzirea unei cladiri rezidentiale sau prepararea apei calde de consum – Revista Romana de Inginerie Civila – volumul 10 (2019) nr.2 – editura Matrixrom, Bucuresti;
2. Florin Iordache, Alexandru Draghici – Procedura de evaluarea a indicatorilor de performanta pentru masini frigorifice sau pompe de caldura - Revista Romana de Inginerie Civila – volumul 10 (2019) nr.4 – editura Matrixrom, Bucuresti;
3. Florin Iordache, Alexandru Draghici, Mugurel Talpiga – Comportamentul Termic dinamic al unei pompe de caldura functionand intre 2 rezervoare de acumulare - Revista Romana de Inginerie Civila – volumul 10 (2019) nr.4 – editura Matrixrom, Bucuresti;
4. Florin Iordache – Modelarea functionarii echipamentelor si sistemelor termice aferente cladirilor – editura Matrixrom, 2021, Bucuresti;
5. Florin Iordache – Alegerea pompelor de caldura pentru alimentarea instalatiilor de incalzire centrala si de prepararea apei calde de consum aferente cladirilor – Revista Romana de Inginerie Civila – volumul 12 (2021) nr.3 – editura Matrixrom, Bucuresti;

Proiectarea unui sistem adaptiv de umbrire solară bazat pe cuboctaedru

Design of adaptive solar shading system based on the Cuboctahedron

Ana-Maria Graur[1].

[1] Technical University of Cluj-Napoca, Faculty of Architecture and Urban Planning.
34-36 Observatorului Street, Cluj-Napoca, Cluj, Romania
E-mail: Anamaria.Graur@arch.utcluj.ro

Abstract. *This paper will develop the design of an interactive, kinetic facade that has the ability to adapt to the intensity of natural light to filter hierarchically, in real time, and prevent visual and thermal discomfort generated by light inside spaces. The purpose of the study is to provide an overview of the main parameters that determine the geometry and design of the system, the kinematic character of the shading system, and also the impact that the kinetic shading system will have on the design of the building facade.*

Keywords: shading envelope, adaptability, kinetic façades, cuboctahedron, hyperbolic paraboloid

DOI: 10.37789/rjce.2022.13.2.6

1. Introduction

Natural light is an essential element of life, it is one of the most significant aesthetic and visual characteristics of architectural spaces, which has a major impact on human physiological and psychological needs. However, it can cause discomfort due to the intensity and overheating of the space.[1] Excessive lighting can cause a number of negative phenomena, among others: photophobia, excessive tearing, pain in the eyeballs, headache. In order to obtain optimal natural lighting, architects and builders must take into account several factors: the orientation of the building in relation to the key points, climate, relief, shape and geometry of the volume, materials used, the vicinity of the building, possible shading of water, the function of the inner spaces and so on.

In the last decades of this century, globally, a series of measures have been taken to stop the waste of natural and financial resources, to limit the harmful effects on the environment, and contemporary architecture is trying to adapt to this requirement by reducing energy consumption. buildings.[2] Changes in the design and image of buildings, with the use of large glazed surfaces outside, allow easy heat transfer, and the comfort of the interior is maintained especially by using mechanical ventilation and air conditioning systems with high energy consumption. These facades

have evolved with technology, and today some are made of many different layers and materials that allow the tire to reconfigure itself to cope with various internal or external changes.[3] From a historical point of view, architecture has always used the natural resources available on the site and has responded to the conditions given by the environment, offering in turn an optimal habitat in relation to the climate. Currently, the trend is to use an adaptable, dynamic building covering, and this receptive architecture is becoming the subject of innovative research studies.[4] Adaptive systems or receptive facades are much more suitable and efficient than fixed ones (blinds, sun visors, etc.), because they can be adjusted according to the change of solar radiation, allowing individual construction, optimal shading and maximizing the use of natural light.[5] By using innovative materials, shape memory alloys, the system can always react the same way, fewer parts are needed and the energy used to operate the shading system is greatly reduced. . The incorporation of several functions at the façade level to optimize the response to various external stimuli is a starting point in this study.

Thus, in this research, I will study the design of an interactive, kinetic facade that has the ability to transform through the dynamic action of light during the day to satisfy the visual and thermal comfort of the interior space. The envelope of the building is the interface between inside and outside, therefore, it significantly influences the indoor climate, comfort and energy consumption of the building and at the same time gives individuality to the building.

2. Design strategy of the sun shading device

The purpose of interactive facade systems is to control the thermal heating or cooling loads of the architectural volume, by controlling the transmission of solar energy at the facade level and at the same time allows control over the visual comfort inside the spaces. Starting from these aspects, I tried to find a way to optimize the shape, the process of transformation and reconfiguration of the elements that which form the shading system, depending on the energy flow to meet the comfort values of users. In order to define the shape of the parasol, the following must be taken into account: the shape of the building and the relationship with the activities of its occupants, climate, orientation of the facade in relation to the cardinal points, shading produced by vegetation or that produced by neighboring buildings. Thus, this interactive facade reflects the fluctuations of the environment and changes its shape in relation to these changes.

Interactive shading systems have a significant potential for integration in the design of fades, and most are the second layer of the facade that interacts with environmental stimuli through several types of movements: rolling, sliding, folding, rotating, etc. can be operated by a sensor activated by an external power source. [6]

2.1 Geometric exploration

As a source of inspiration in the creation of the shading system, the generation of modules based on the spatial structure and geometry of regular polyhedra was explored, so that the modules could be interconnected to generate a network. Due to the possibility of linking, in future studies, the digital model to the parameters of natural light, it was decided to use the Rhino 7 program. Thus, the variety of semi-regular polyhedra, the 13 Archimedean solids, provides an infinite source of new architectural forms both through their individual multiplication and the combinations of several. All these volumes have a perfect symmetrical shape, which represents a very good source of inspiration for builders and architects. Polyhedra that can be joined together to fill the space exactly with no gaps, so that every face of each polyhedron belongs to another polyhedron, may be thought of as cells in a space-filling honeycomb.[7] In order to obtain a greater diversity and dynamics universal laws and principles can be reproduced, such as the asymmetry resulting from the repetition and the combination of some of the volumes. The flat surfaces of the semi-regular polyhedra thus assembled are perfect for overlapping or joining.

From all the semi-regular polyhedra the cuboctahedron was chosen because it offers through the section with a plane passing through the center of the polyhedron and the edges of the cuboctahedron a hexagon that allows the creation of a network of hexagons. Figure 1 shows the cuboctahedron in a sequence of changes in projection planes for a clearer view of the polyhedron.

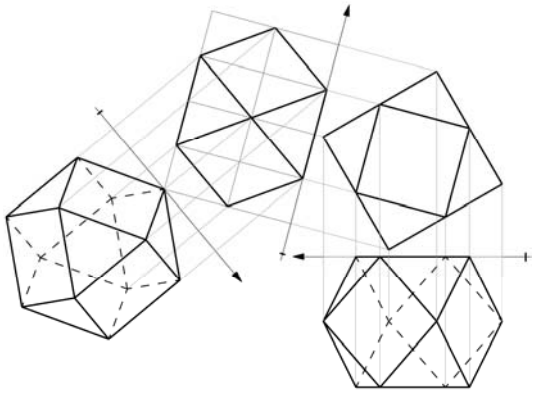

Fig. 1. Geometric representation of the Cuboctahedron

A cuboctahedron is a polyhedron with 8 triangular faces and 6 square faces and he has 12 identical vertices, with 2 triangles and 2 squares meeting at each, and 24 identical edges, each separating a triangle from a square. For any pair of vertices, there is a symmetry of the polyhedron that transforms one vertex to another. It is the only radially equilateral convex polyhedron. This polyhedron is obtained by successively cutting off each of the vertices of the octahedron or cube. [8]

However, in order to be able to generate the shading module, three-dimensional continuous minimum surfaces have been aggregated that generate hyperbolic paraboloids between the edges of the three equilateral triangles that form the hexagon

and then investigate how these geometries can be modeled to optimize surface displacements. As we know the hyperbolic paraboloid or crooked plane is a smooth surface that is obtained by moving a straight generator in two directions, which are all straight, uncoplanar, movement during which the right generator remains parallel to a given master plane, Figure 2.

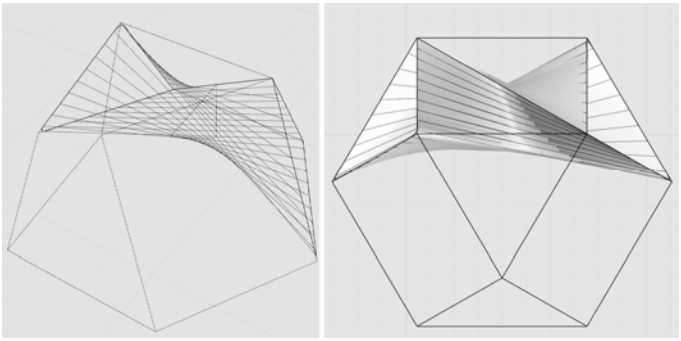

Fig. 2. The use of hyperbolic paraboloid in design of solar shading module

The connection between two hyperbolic paraboloids is made with a small portion of the cylindroid. The cylindricalroid is a directed surface with a directional plane whose generator rests on two directional curves not located in the same plane, remaining parallel to a given plane.[9] In these terms, the design of the light-sensitive sun visor will continue by making different ways of rotating surfaces, exploring the type of hyperbolic paraboloids that generate various curves, Figure 3 and use smart materials as actuators.

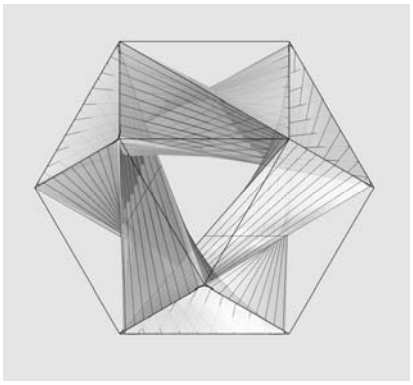

Fig. 3. The view of the solar shading module

2.2 Dynamic characteristics of sun shading device

In this section we will analyze the way in which the movement of the module in the shading system can be achieved, through which the internal lighting and the thermal comfort of the architectural space can be controlled.

Complex drive systems are an unfavorable solution, as the energy required to drive should cost as little as possible. A mechanically operated system is more expensive and requires permanent maintenance to reduce the occurrence of faults. But

looking at the architectural context, I noticed that the whole system becomes an integral part of the facade and will influence the overall design of the building, being important to choose drive systems with a design as pleasant as possible. Consequently, the number of actuation points, the required displacements and the actuating forces are important parameters that must be taken into account in the design phase to ensure the sustainability of the systems, so the use of shape memory materials has been considered.

Thermally, SMAs are designed to change shape when the temperature rises to 50-70 ° C (depending on the alloy). As the shading system should be guaranteed throughout the year, the operation of the SMA would be more likely to be activated by a power source. [10] The elasticity of the material results in different types of geometric transformations.

Thus, the deformation process of the solar shading module is performed by rotating to the left or to the right by 28° in relation to the initial position of the equilateral triangle in the level plane with the highest elevation and results in the modification of adjacent surfaces, more precisely, the saddle surfaces of the hyperbolic paraboloids what composes the system, and thus results a modified spatial structure of the cuboctahedron. This three-dimensional structure implicitly provides self-shading, and the planes of the saddle surfaces of hyperbolic paraboloids allow the diffusion and redirection of sunlight.

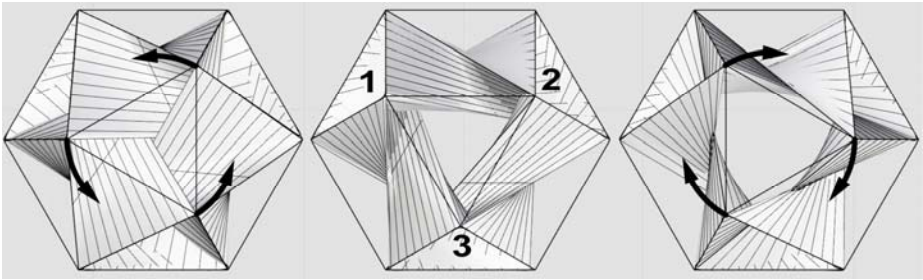

Fig. 4. The phases of solar shading module types

Figure 4 shows how the deformation is generated by pushing points 1, 2 and 3, forcing the surfaces of the hyperbolic paraboloids to change their curvature, to close or to open the free surface between them. The arrows shown in the image indicate the orientation of the actuator. The extension and retraction of the elements, which connect the hexagon and the equilateral triangle located in the level plane, are the movements sought in the generation of this receptive structure.

2.3 Intermediate positions of sun shading device

Reducing the brightness and controlling the thermal energy of natural light in real time are the objectives developed by the design of the proposed shading system. Normally the system uses several phases in the movement process to adapt to the dynamic light of day.

Modifying the radius of rotation of the equilateral triangle by extending and retracting some edges of the cuboctahedron can vary the actuation in this model to generate the opening and closing of the module in the shading system.

To take into account the future development of physical prototypes, digital experimentation has taken into account the spatial structure of the entire system, which also involves anchor points.

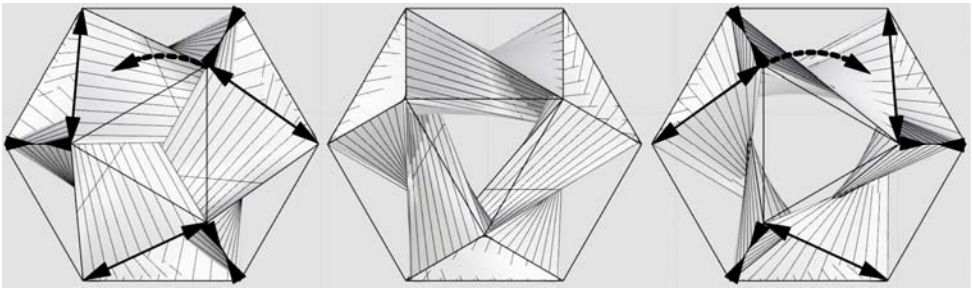

Fig. 5. The phases of solar shading module types

These fixed anchor points are located in the hexagon plane and determine the constraints of the module movement, by twisting the equilateral triangle in the level plane. As shown in Figure 5, the tips and edges operate the entire module for closing or opening, by rotating the equilateral triangle between 0° (initial position, middle figure) and 28° on a two-dimensional surface, providing real-time control of the facade over fluctuations of light intensity and a wide range of intermediate positions. Figure 6 shows spatially some intermediate positions of the shading module.

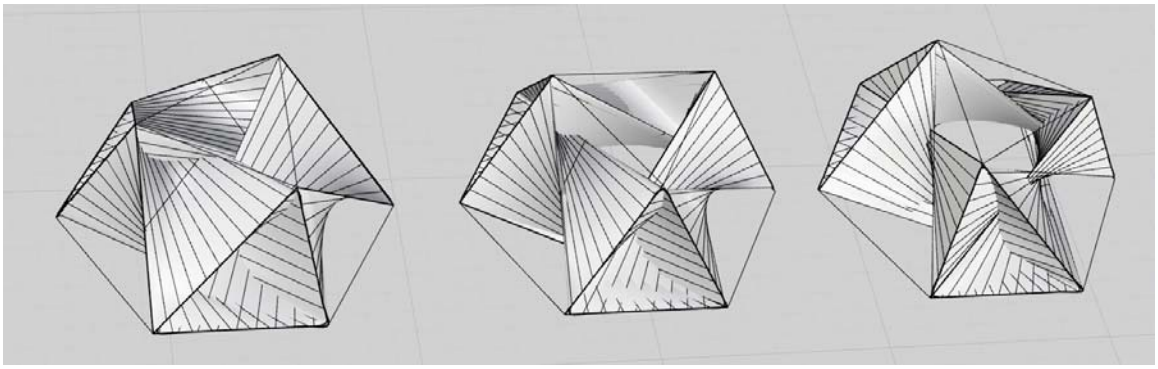

Fig. 6. the perspective view of the solar shading module

3. The impact of the kinetic shading system in the design of the building facade

Over time, architectural thinking has evolved from stability to dynamism and movement, being stimulated by ternological progress, computer-aided design and new building materials. The envelope of the building is the place where the architecture is expressed to the outside, to the public, but also the place that must mediate energy and structural problems, the boundary between interior and exterior conditions, being often

considered a two-dimensional surface and less a component of the three-dimensional building, more likely, stratified.

Using the octahedron as the spatial structure and the hyperbolic paraboloid as the connecting surface we have the possibility to generate an adaptable system that can be integrated in the design of the receptive shading elements. Through the proposed design for this shading system, the geometry of the facade is changed due to the kinetic structure, which responds passively to the fluctuations of light intensity. This vibrant movement in the facade of the building changes the image of the architectural volume through the intelligent materials used as actuators of the system, which offers, at the same time, the possibility to act the individual each module. Thus, if the neighboring module responds to the movement of the first one, the fluid effect of a flock of starlings, known as the murmuration of starlings, can occur. The result is gaps with various openings, which in turn generate ingenious dynamic compositions and texture the vertical planes with three-dimensional shapes. The permissive and vibrant envelope, through the attributes of the surface shape, is dynamic and semi-transparent through these variable gaps of the moving modules assembled in this way, Figure 7, with a view of the whole in the direction of the interior space.

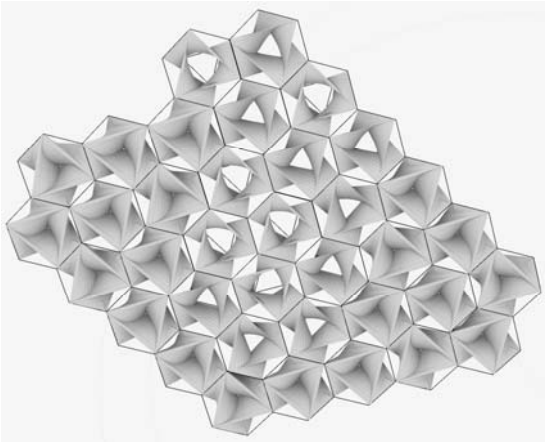

Fig. 7. Solar shading modules assembled - view from the direction of the interior space

The modern facades of buildings, with complex shapes, have geometric and mechanical limits in the realization of shading systems, but an advantage of this system is that it is modular and adapts to a design with flat facades and one with more complex shapes. This shading system makes it very easy to generate a space frame structure, a hexagonal matrix capable of withstanding structural stress. The points where the shading system is operated are integrated in the structure of the module, this semi-cuboctahedron, having a major influence in the general architectural expression of the building, as seen in Figure 8, with a view of the whole from the outside.

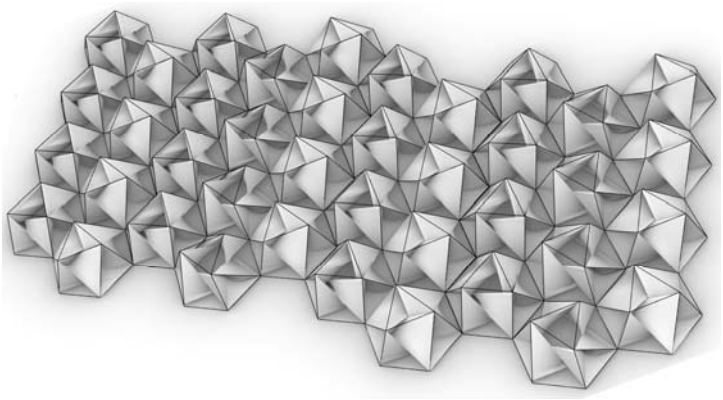

Fig. 8. Solar shading modules assembled - view from the direction of the exterior space

By choosing materials with different light transmitting properties, the interior space will be protected by dynamic elements capable of filtering solar radiation throughout the year and generating a new atmosphere and, of course, meet the requirements of visual comfort due to the design of the facade. By choosing the right materials, this three-dimensional structure can contribute to the diffusion and redirection of the sun's rays. In the future we can consider storing solar energy by using this type of solar shading modules and the right materials for this process.[11]

This study discusses a permissive, spatial, perforated and vibrant envelope through the rhythm given by the modulation of the kinetic shading system, which can contribute positively to the design of a building with flat facades. In Figure 9 you can see a variant of assembling the module as a shadow system, seen from inside and outside.

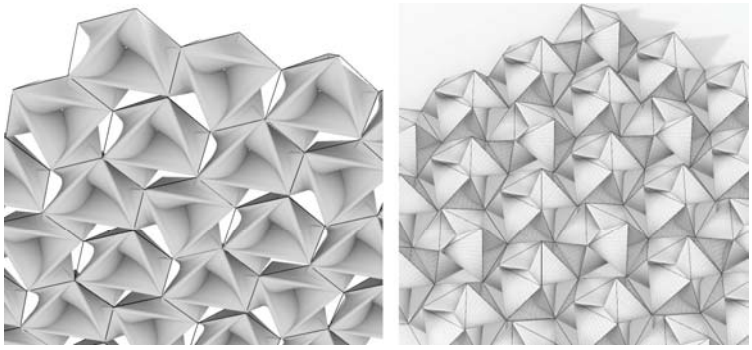

Fig. 9. Solar shading modules assembled

To do architecture means to study, among other things, the way light enters, the way you see the surroundings and this is exactly what we can capitalize on through this envelope. We can generate, so to speak, a film, which focuses your gaze on various interesting exterior perspectives, premeditated in the design phase, and the play of light that enters to animate the interior spaces by moving the whole system, Figure 10.

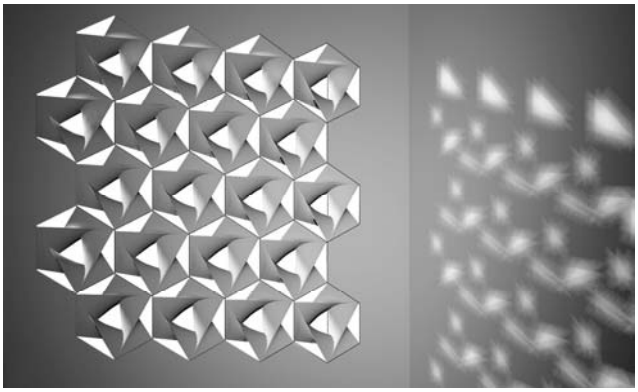

Fig. 10. Solar shading modules assembled

4. Conclusion

The design of a receptive envelope that allows the shading of the building, represents the continuous optimization of the parameters that come from the interior and exterior space, thus improving the thermal and visual values inside the building. As a result, the half-octahedron kinetic modular elements diffuse daylight through three-dimensional configurations of parabolic hyperboloids, providing self-shading of the façade, decreasing the intensity of direct solar radiation and allowing optimal natural light to enter the interior, helping to reduce energy consumption and an increase in the autonomy of natural light. The receptive façade useful for improving the comfort of the interior space is still being developed and represents a new trend in architectural design. Starting from the idea of using shape memory alloys as system actuators to reduce the actuation energy, the research will study how the whole assembly works and how we can improve the shading device included in the layers of a tire.

There are several possibilities for how the research undertaken in this paper could progress in the future, and with the evolution of technologies to adapt the system to a more complex and implicit, improving its performance. For example, the next step would be to apply this logic to a real envelope and study the feasibility and performance of natural light in a prototype experimental research and then study the direct relationship between the occupants of these spaces and the interactive movement of the shading system. This step involves a parametric design approach. The geometry of this facade, surfaces with angles inclined or oriented in a certain direction, offers the opportunity to capitalize on the potential for capturing and using solar energy. This study is intended to serve as a guide for future research in the field of intelligent architecture.

References

[1] Stephen M. Pauley, „Lighting for the human circadian clock: recent research indicates that lighting has become a public health”, Medical Hypotheses, Volume 63, Issue 4, ISSN 0306-9877, pp. 588-596, 2004.

[2] Directive 2010/31/EU of the European Parliament and of the Council on 19 May 2010 on the energy performance of buildings [2010] OJ L153/13
[3] Bohnenberger, S., Khoo, C.K., Davis, D., Thomsen, M.R., Karmon, A., Burry, M. „Sensing Material Systems-Novel Design Strategies". International Journal of Architectural Computing, Volume 10, Issue 3, ISSN 2048-3988, pp. 361-376, 2012.
[4] Khoo, C.K., Burry, J., Burry, M. Soft Responsive „Kinetic System: An Elastic Transformable Architectural Skin for Climatic and Visual Control". ACADIA 11: Integration through Computation [Proceedings of the 31st Annual Conference of the Association for Computer Aided Design in Architecture (ACADIA)] [ISBN 978-1-6136-4595-6], pp. 334-341, 2011.
[5] Schnittich, C., Krippner, R., Lang, W. „Building Skins, Detail", Birkhäuser, Basel, 2012.
[6] Hosseini, S.M., Mohammadi, M., Guerra-Santin, O. „Interactive kinetic façade: Improving visual comfort based on dynamic daylight and occupant's positions by 2D and 3D shape changes", Building and Environment, Volume 165, ISSN 0360-1323, 2019.
[7] Viana, V. „From Solid to Plane Tessellations, and Back". Nexus Network Journal Volume 20, pp. 741–768, 2018.
[8] Graur, A.M. „Geometry as assembly in architecture. Semi-regular polyhedra". Journal of Industrial Design and Engineering Graphics, Vol. 15, Iss. 2, pp. 17-20, 2020.
[9] Iancau, V., Barbat, V., Rusu, I., Zetea, E., Rosa, S., „Geometric representations and technical drawing", Publisher Didactics and Pedagogics, Romania, pp. 220-223, 1982.
[10] Pesenti, M., Masera, G., Fiorito, F., „Sauchelli, M., Kinetic Solar Skin: A Responsive Folding Technique", Energy Procedia, Volume 70, pp 661-672, 2015.
[11] Mârza, C., Corsiuc, G., „Considerations on solar energy storage", Bulletin of the Transilvania University of Braşov • Vol. 10 (59) Special Issue No. 1, pp.390-397, 2017.